Chapter 5

Thermoluminescence of Strontium Pyrophosphate

5.1. Introduction

In this chapter, the basic information of thermoluminescence (TL) is described in detail. The principle of thermoluminescence, theoretical background and TL mechanism, methods for TL parameters estimation, instrumentation of TL reader, etc are explained briefly. Chapter contains experimental results and discussion of thermoluminescence property of rare earth doped strontium pyrophosphate after beta irradiation. Characterization study of the TL glow curves have been done by evaluating the kinetic parameters, activation energy, and frequency factor using several standard analytical methods of TL analysis. Outcome of TL results has been discussed on the basis of theory and its application in detail.

5.2. Thermoluminescence

5.2.1. Overview

Thermoluminescence (TL) is a very old discovery which can initiated by scientists Robert Boyle. The concept of thermoluminescence was first observed by Robert Boyle in 1663 [1-3]. He reported to the Royal Society about observation 'glimmering light' emitted from a diamond upon a warming it by his part of ‘Naked Body' that reveals the phenomenon of thermoluminescence [4, 5]. He observed similar light emission from the diamond by using more conventional sources of heat like a hot iron, friction and candle. Elsholtz (1676) observed such kind of result from the fluorspar mineral [6]. The earliest explanations of such phenomena were given in form ‘the heat itself was being directly converted into light’. Oldenburg (1676), termed the thermoluminescence phenomenon of a phosphor as ‘the material received its light from the fire itself’ [7, 8]. Majority of such kind of other observations at that time supported this concept. DuFay (1726) paying attention that the luminescence observed in ‘sulphur’ was due to actually burning of sulphur on heating [6]. After word, he was mentioned that the observed phenomenon (i.e., thermoluminescence) was nothing but the delayed phosphorescence and stated ‘Heat only stimulated the emission, but was not its cause’ (DuFay, 1738) [1]. He is performed similar experiments on natural quartz and conclude that the thermoluminescence from the quartz could be initiated by exposure of the sample to light [9]. Other well-known scientists De Saussure and Thomas Wedgwood also mentioned the thermoluminescence studied of the eighteenth

century [10, 11]. They former recognized several types of stones like sulphur or a hepar, dolomite and fluorspar were luminescent on heating [12].

Heinrich stated that more or less all material could emit light, the material should be in powder form and it should be subject under reasonable heating [13, 14]. Theodor von Grotthus dealt researched particularly with the fluorspar material, and explain similar concept take place in between thermoluminescence and essence, he proposed both are made of positive and negative parts [15]. Afterwards, scientist David Brewster conflicted to Grotthus's concept [6]. He made arguing that the luminescence property of materials cannot forever be regained on exposing the material to light [1, 15]. Pearsall attempted to find out the correlation between colour and thermoluminescence [13]. Most extensively useful application of thermoluminescence as used now a day in TLD can be first traced back to experiments by Wiedemann and Schmidt (1895) [1, 16]. They were extensively studied a broad range of inorganic substances and natural minerals, using a beam of cathode ray for the initial irradiation of the phosphors [17, 18]. Trowbridge & Burbank (1898) perform an experiment by draining the natural thermoluminescence from fluorite mineral by heating and then again re-excited the thermoluminescence in fluorite by exposing it to X-rays [13, 19]. Madame Curie (1904) studied the radiation-induced thermoluminescence properties of fluorite, which boost up the phenomenon of radiation-induced thermoluminescence. Marie Curie (1904) wrote her doctoral thesis on: ''*Certain bodies such as fluorite, becoming luminous when heated. Their luminosity disappears after some time, but the capacity of becoming luminous afresh through heat is restored to them by the action of a spark and also by the action of radiation*'' [20, 21]. Urbach (1930) experiments to study TL from alkali halides, suggested that the temperature at which the maximum TL peak occurs is depends on the electron trap depth [22, 23].

The fundamentals of TL theory come into view due to Randall and Wilkins (1945) and Garlick and Gibson (1948) [13, 15, 21, 24]. They established the mathematical expressions for the shape of a TL glow peak resulting in terms of temperature, radiation dose, heating rate, and the characteristic of the different types of trap [1]. Thermoluminescence materials, TL mechanisms, and application of TL in various field like including dosimetry, radiation damage, studies of catalysis, TL stratigraphy, identification of minerals, age determination of rocks and pottery has been widely discussed by Daniels (1953) [21, 25].

There are large number of natural minerals like quartz, calcite, flint and feldspar emit light whenever warming upon heat. The phenomenon of TL was not only sufficient to be used for study a dating method. It was more essential to establish the TL mechanisms. After very long time about three centuries later the first law of thermoluminescence was recognized to explain TL mechanism [12]. Roth et al, 1989 states that TL intensity is approximately proportional to the irradiation dose given to the material [26, 27].

Recently, application of thermoluminescence is found very precious in many scientific disciplines. The applications include personal dosimetry, environmental and retrospective dosimetry, geological and archaeological dating, and in a variety of medical applications such as radiation therapy, diagnostic radiology and radiotherapy dosimetry [28-31]. For diagnostic radiology, a dosimeter with a flat energy response to low energy photons is preferred. In archaeology (for dating ancient pottery) using the accumulation of background irradiation dose in TL material within the clay which the pottery is made of and solid state research as a tool to investigate defects in insulators and semiconductors [32, 33]. The background of the research described in this thesis is the interest in dosimetry applications of thermoluminescence.

5.2.2. Principle

The conventional explanation of Thermoluminescence (TL) also called as thermally stimulated luminescence (TSL) is the phenomenon of emission of light occurring from materials having large energy gap like the insulators or semiconductors invoked the absorption of energy from an ionizing radiation source [13, 34]. The absorption of radiation energy results into the excitation of free electrons and free holes. The successive trapping of these electrons and holes occur at defects or trapping states within the energy gap of the material. The emission of light occurs when the material is heated subsequently after removal of the excitation [35]. The thermal energy is used to liberate the charge carriers of negative sign i.e., electrons which are then recombine with charge carriers of the positive sign i.e., holes. If the emission occurs due to recombination process of electron is radiative, the emission is termed as thermoluminescence (TL) [36]. The basic description of TL phenomenon can be given in the following statement which is very similar to the thermally stimulated luminescence (TSL) phenomena: "*TL requires the perturbation of the system from a state of thermodynamic equilibrium, via the absorption of external energy, into a*

metastable state. This is then followed by the thermally stimulated relaxation of the system back to its equilibrium condition" [1].

In the definite case of TL, the perturbation process is generally the absorption of energy from ionizing radiation, and then the thermally stimulated relaxation (TSR) back to equilibrium, which is followed by monitoring the radiative emission of luminescence from the system during the transitions of the freed charges back to the ground state [6, 37]. The TL intensity of the emitted luminescence is associated to the rate at which the system returns to equilibrium [38].

TL phenomenon is observed in a variety of synthetically produced solid states materials, such as semiconductors, metallo-organic compounds, organic solids, and also in complex biological systems like the photosynthetic materials [12]. A familiar characteristic of TL phenomena is the storage of radiation energy in metastable trap states formed in energy gap, which can be further released via thermally stimulated radiative detraping [39].

5.2.3. TL Mechanism

Basic theoretical concept of pure crystalline luminescence materials normally established is mainly based on the ‘‘collective electron" model of Bloch which has been accepted by many researchers. The allowed energy levels formed for electrons in such type of phosphors made up of bands structure of energy states separated by forbidden energy bands in which the outermost electrons of atoms are responsible for luminescence processes [40, 41]. In ideal crystal lattice the lattice defects, impurity and other perturbations can induce the discrete energy levels similar that of an isolated atom which can lie in the forbidden energy region [42]. In some other type of phosphors, impurity ions or larger complexes agents can take part as luminescence emission centres at the discrete energy levels by providing electron trapping energy levels just below the conduction band of the semiconducting or insulating system [43, 44]. The energy levels introduced in forbidden gap may be discrete or distributed which is depending on the nature of the defect and the host lattice. Such types of electron traps inside the forbidden gap have been considered to be responsible for the phenomenon of phosphorescence and thermoluminescence taking place inside phosphors [11, 14].

During the excitation the electron released from the valence band which could be travelling throughout the crystal may become 'trapped' inside hole due to Coulombian field attraction of a unoccupied anion site which cannot able to take part in

conduction for long time [45, 46]. The minimum energy required to release such electron from the trap center is much less than that of the energy required for freeing a valence electron, therefore the anion vacancy can create metastable energy level between the valence and the conduction bands [47]. A similar type of energy levels can arise due to cation vacancies where the missing cation creates a deficiency of positive charge called as hole, as a result the energy require for free an electron from the neighbouring anion can decrease. Anion and cation vacancy in crystal structure are responsible for the formation of localized energy levels inside the forbidden gap [48]. The arrangement of the localized energy levels inside the forbidden gap is determined by the decrease in the energy required to free the electron from the particular energy level [49]. The energy level arise due to the anion vacancies have an energy more than that of the Fermi energy as a result such energy level positioned above the Fermi energy level and are empty of electrons which can potential electron traps [50]. Similarly the energy level arise due to the cation vacancies have an energy less than that of the Fermi energy as a result such energy level situated bellow the Fermi energy level and are full of electron which can potential hole traps [50]. Similar kind of condition has been take place under the incorporation of substitutional or interstitial impurity ions formed within the crystal lattice. The introductory energy band diagram for an insulator or semiconductor containing electron and hole trapping levels is shown in Figure 5.1.

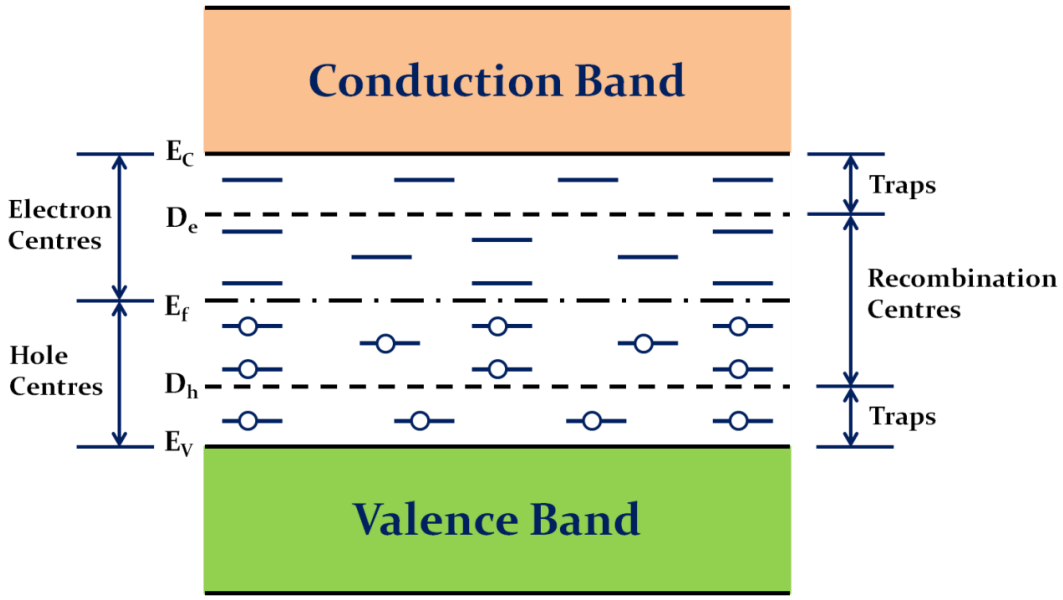

Figure 5.1 Energy levels diagram of an insulator and semiconductor at absolute zero temperature [1].

The mechanism of TL model in large band gap material is based band theory. According to this theory the ionizing radiation energy is absorbed which generate free electrons, holes and defects in the material [14]. Following processes are take place in the TL mechanism:

- ***Trapping by luminescent centres (LCs):*** Different type of impurity ion can form electron or hole traps in energy gap with a free charge carrier (i.e., electron or hole). The emission of a photon (radiative recombination) can take place if the opposite charge can reaches to the filled the empty trap and recombines with the previously trapped charge. The emission of photons mainly depends on the characteristics of the impurity ion [14, 48, 51-53].
- ***Trapping by non-radiative centres:*** The free charge carriers (cation/anion) can form the bound states not only with luminescence centres, but also with other various ions/molecular ions. The basic characteristic nature of band states cannot remains same, it could be frequently change. When the charge carrier of the opposite sign arrives to fill the trap, it recombines with the previously trapped charge, but the released energy dissipates without emission of photons (non-radiative recombination) [52, 54, 55].
- ***Mutual recombination:*** Some of the free charge carriers of opposite signs can recombine in the matrix without trapping by luminescence centres and non-radiative centres [6, 14, 41, 54].
- *Free charges can be recombine with defects of opposite charge at trapping centres via both radiative and non-radiative transition* [6, 14, 52-55].
- ***Thermal activation ejection of electrons and holes from traps:*** The trapped electrons and holes form a bound state with a trapping centres at different enegy level. The binding energy of this trapping centres can determines the lifetime or the disintegration probability of the bound state. The disintegration probability increases with increasing temperature [6, 14, 53].
- ***Redistribution of electrons and holes between traps and luminescence centres due to thermal excitation into conduction and valence bands:*** The charge carriers can produce due to thermal activation from filled traps in the system can be retrapped by all other empty traps, i.e. both luminescence centres and non-radiative centres [14, 44, 55].

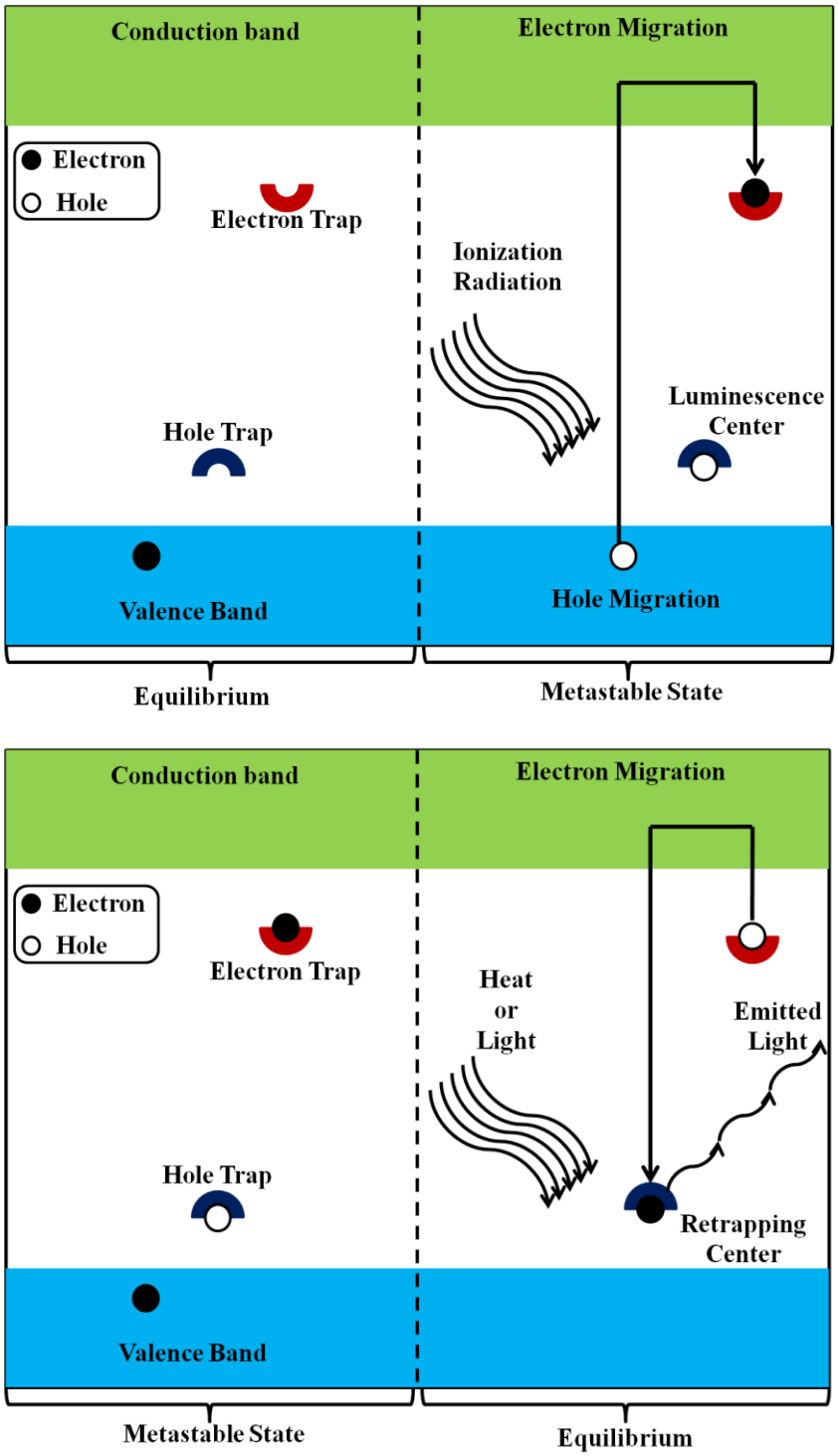

Figure 5.2 (a) Energy-level diagram of the energy storage stage for TL processes; (b) Energy-level diagram of the energy release stage for TL processes.

Figure 5.2(a) shows the mechanism of the irradiation energy storage process by the electron-hole pair creation and excitation. When the phosphor irradiated by some ionization radiation, the electrons inside the valence band can excited to the conduction band as a result hole forms in the valence band [56]. The excited electron cannot

remains stationary in conduction band and find the way to accumulate into an electron trap as well as the holes can also occupies into its related trap. In this process the hole traps are termed as the luminescence centres [57, 58]. Figure 5.2(b) shows the thermoluminescence process. In which trapped electron can release the sored energy by emission of photon when the temperature raise. In this process the trapped electron is released through conduction band and retrapped with the hole trap called as recombination center [6, 13].

5.2.4. Methods for TL parameter

The main objective to study thermoluminescence experiment is to find out the important data from an experimental TL glow-curve. Various informative TL parameters can be found using these data which is very useful to understand the mechanism associated with the charge transfer process takes place in the material under study [59, 60]. The TL parameters like the trap depths (activation energy) 'E_a', the frequency factors 's', the densities of the various traps and recombine at ion centres taking part in the thermoluminescence emission [13, 61]. Many theoretical approaches have been done to determine TL parameters on the basis of some assumptions. The most accepted method for evaluate TL parameters can begin by choosing appropriate rate equations for a particular band model by introducing some simple assumptions. The modified rate equations after some assumptions can be used as an analytical expression which significantly describes the variation in thermoluminescence intensity with temperature in terms of the required parameters [62, 63]. In this procedure, the first assumption is taken into consideration such that the model is used to describe the thermoluminescence production and the second assumption is taken into consideration in rate equation which can be certainly limits the generality and possibly the validity of the obtained results from glow curve [1, 64, 65].

To evaluate the TL parameters, several methods have been used to evaluate the TL glow-curve, and the results obtained from the diverse methods have been compared with each other to estimate outcome of glow curve. Initial rise (IR) method, peak shape methods (PSM), Kitis et al. equation for curve fitting (GCD fitting), and whole glow curve-peak method have been used to determine TL parameters [66].

5.2.4.1. Initial Rise (IR) Method

Initial rise method is been recognized by Garlick & Gibson (1969), where they considered the intensity of initial rise part of a TL glow-curve or the rate of change of

the trapped carrier concentration is exponentially dependent on temperature according to the relation [11],

$$I(t) = -\frac{dn}{dt} = (constant) \times exp\left(-\frac{E_a}{k_B T}\right) \dots\dots\dots\dots\dots\dots\dots\dots (1)$$

This equation termed as if the heating temperature of the sample is low enough, the trapped carrier concentration 'n' to be remains approximately constant because of very small amount of detrapping have taken place [41]. This relation is independent of the order of kinetics of TL mechanism. The essential condition for initial rise method is that 'n' remains approximately constant if the increase in temperature of sample beyond a critical temperature 'T_C' than this assumption becomes invalid [36, 58, 67]. The critical temperature 'T_C' corresponds to the TL intensity 'I_C' less than 10-15% of the maximum TL intensity. Initially occupancy of traps and recombination centres are assumed to be remains constant only up to a limiting temperature range under 'T_C' [63, 68]. If a plot of ln(I) versus $1/k_BT$) is made for the initial rise region, a linear function with a slope of (E_a/k_B) from which the activation energy E_a is simply determined, while the intercept on the ln(I) axis of the plot gives ln(s/β) which the frequency factor 's' is found. Here, E_a is the activation energy, k_B is the Boltzmann's constant and T is the temperature, β is heating rate. The activation energy obtained from this method cannot be the true valued [68-70].

5.2.4.2. Whole Glow-Peak Method

In initial rise method, TL parameter has been calculated using only the limited data of the initial rising region which is severely limited condition for analysis. This difficulty can be overcome by using the whole curve data for evaluate TL parameters. Chen and McKeever proposed a simple model to give explanation of the basic TL phenomenon [13, 29, 57]. According to this model, the number of electrons released per second is proportional to the total concentration of trapped electrons. This means that there is no retrapping of electrons from the conduction band [14, 71]. From these assumptions, the rate of production of emitted photons or intensity I(T) of TL for second order kinetic is given by

$$I(T) = -\frac{dn}{dt} = n^2 \frac{s}{N} exp\left(-\frac{E_a}{kT}\right) \dots\dots\dots\dots\dots\dots\dots\dots\dots\dots\dots\dots (2)$$

The whole glow-peak method yields information about the activation energy E_a and the effective frequency factor $s'=s/N$ from bellow expression [61, 72].

$$I(T) = n_0^b \frac{s}{N} exp\left(-\frac{E_a}{kT}\right)\left[1 + \frac{n_0 s}{\beta N}\int_{T_0}^{T} exp\left(-\frac{E_a}{kT'}\right)dT'\right]^{-b} \ldots\ldots(3)$$

Where, n_o is the area under active curve, b is the order of kinetics (1.8, 1.9, 2.0, 2.1), (s/N) = s' is the frequency factor, k_B is the Boltzmann's constant, β is the heating rate, and E_a is the activation energy [61, 62, 65]. In whole curve method, a plot of $\ln[I(T)/nb]$ versus $1/T$ gives a straight line having slope ($-E_a/k_B$), and an intercept of ln (s'/β). The straight line can be obtained by putting the proper value of b in above equation [73]. The major difficulties came about to use whole curve method is that it requires merely isolation glow peaks and a clean descending part of the last peak in the glow-curve [1, 57].

5.2.4.3. Peak Shape Method

Peak shape method (PSM) used for analysis of the glow-curve can just utilize three points of the TL glow-curve rather than the partial or whole peak analysis methods, because of the shape of glow-peak is mainly affected by the order of kinetics as a result the method strongly dependent on the order of kinetics [13, 25, 74]. Chen developed the PSM for general-order kinetics using the (Halperin & Braner, 1960) geometrical factor defined as $\mu_g = \delta/\omega$ and solved the general-order equation for thermoluminescence [73, 75]. The values of geometrical factor μ_g for the first-order kinetics and second-order kinetics are 0.42 and 0.52, respectively while for the general-order kinetics the geometrical factor μ_g is seen to vary from 0.42 to 0.52 [6, 60, 76].

TL parameters have been easily calculated using the Chen's peak shape method. Chen(1969) proposed three equations for both first-order kinetics, second-order kinetics and general-order kinetics [76]. The TL parameters of the glow-curves have been calculated using three parameters τ, δ and ω.

$\tau = T_M - T_1$ $\quad$ $\delta = T_2 - T_M$ $\quad$ $\omega = T_2 - T_1$

Where, 'τ' is the low temperature half width of a peak, 'δ' is the half width at the high temperature and 'ω' is the total half-intensity width. T_1 and T_2 are the low and high temperatures corresponding to half-maximum intensity, respectively [6, 13, 60]. T_M is the temperature at maximum intensity. Three equations of activation energy for τ, ω and δ are given by [13, 63, 64, 77]:

For first-order kinetics:

$$E_\tau = \frac{1.51kT_M^2}{\tau} - 1.58(2k_BT_M) \ldots\ldots\ldots\ldots\ldots\ldots\ldots\ldots\ldots\ldots\ldots\ldots\ldots\ldots(4)$$

$$E_\delta = \frac{0.976 k_B T_M^2}{\delta} \ldots\ldots (5)$$

$$E_\omega = \frac{2.52 k_B T_M^2}{\omega} - 2kT_M \ldots\ldots (6)$$

For second-order kinetics:

$$E_\tau = \frac{1.81 k_B T_M^2}{\tau} - 2(2kT_M) \ldots\ldots (7)$$

$$E_\delta = \frac{1.71 k_B T_M^2}{\delta} \ldots\ldots (8)$$

$$E_\omega = \frac{3.54 k_B T_M^2}{\omega} - 2kT_M \ldots\ldots (9)$$

For general-order kinetics:

$$E_\tau = \frac{1.72 k_B T_M^2}{\tau} - 1.874(2kT_M) \ldots\ldots (10)$$

$$E_\delta = \frac{1.487 k_B T_M^2}{\delta} \ldots\ldots (11)$$

$$E_\omega = \frac{3.234 k_B T_M^2}{\omega} - 2kT_M \ldots\ldots (12)$$

Where E_τ, E_ω and E_δ are the activation energy of TL glow curve for the three temperature co-efficient τ, ω and δ.

5.2.4.4. Glow Curve Deconvolution (GCD) Method

The analysis of composite TL glow curve have been done by the glow-curve deconvolution (GCD) technique, in which the whole curve is divided into the individual glow peaks [78]. The TL glow curves are analysed by using the glow curve deconvolution (GCD) method developed by Kitis et al [79]. This method can used for first-order kinetics, second-order kinetics and general-order kinetics TL glow curves. The mathematical expression for different kinetics of TL glow curve are mainly depends on two experimentally measured parameters, one of them is the maximum TL intensity 'I_M' and another is the temperature corresponding to the maximum TL intensity 'T_M' [63, 78-80].

Kitis, et al equation for first-order kinetics:

$$I(T) = I_M \exp\left[1 + \frac{E_a}{k_B T} \cdot \frac{T - T_M}{T_M} - \frac{T^2}{T_M^2} \times \left(1 - \frac{2k_B T}{E_a}\right) exp\left(\frac{E_a}{k_B T} \cdot \frac{T - T_M}{T_M}\right) - \frac{2k_B T_M}{E_a}\right] \ldots\ldots (13)$$

Kitis, et al equation for second-order kinetics:

$$I(T) = 4I_M exp\left(\frac{E_a}{k_B T} \cdot \frac{T - T_M}{T_M}\right) \times \left[\frac{T^2}{T_M^2} \cdot \left(1 - \frac{2k_B T}{E_a}\right) exp\left(\frac{E_a}{k_B T} \cdot \frac{T - T_M}{T_M}\right) + 1 + \frac{2k_B T_M}{E_a}\right]^{-2} \quad \ldots\ldots\ldots\ldots\ldots\ldots\ldots\ldots\ldots\ldots\ldots\ldots\ldots\ldots\ldots\ldots\ldots\ldots\ldots\ldots (14)$$

Kitis, et al equation for general-order kinetics:

$$I(T) = I_M b^{b-1} exp\left(\frac{E_a}{k_B T} \cdot \frac{T - T_M}{T_M}\right) \times \left[(b-1)\frac{T^2}{T_M^2} \cdot \left(1 - \frac{2k_B T}{E_a}\right) exp\left(\frac{E_a}{k_B T} \cdot \frac{T - T_M}{T_M}\right) + 1 + -1)\frac{2k_B T_M}{E_a}\right]^{-\frac{b}{b-1}} \quad \ldots\ldots\ldots\ldots\ldots\ldots\ldots\ldots\ldots\ldots\ldots\ldots\ldots\ldots\ldots\ldots\ldots\ldots\ldots\ldots (15)$$

Where, T_M is the maximum temperature corresponding to I_M, T is the temperature TL data, k_B is the Boltzmann's constant and E_a is the activation energy. The TL intensity obtained theoretically for different activation energy from the experimental data has been compared and the excellent fitting have been done in GCD method. The precise fitting of experimental TL glow curve and theoretical TL glow curve is been determined by calculating the figure of merit (FOM).

The FOM is obtained by the bellow the relation:

$$FOM = \frac{\sum_p |I_{Exp} - I_{Th}|}{\sum_p |I_{Th}|} \quad \ldots\ldots\ldots\ldots\ldots\ldots\ldots\ldots\ldots\ldots\ldots\ldots\ldots\ldots\ldots\ldots\ldots\ldots\ldots\ldots\ldots\ldots\ldots\ldots\ldots\ldots (16)$$

The frequency factor (s) of TL glow curve has been calculated by using the proper value of activation energy E_a of that glow peak for which the curve fitting is the most precise.

Frequency factor of first order kinetics is obtained by the bellow the relation:

$$s = \frac{\beta E_a}{k_B T_M^2} exp\left(\frac{E_a}{k_B T_M}\right) \quad \ldots\ldots\ldots\ldots\ldots\ldots\ldots\ldots\ldots\ldots\ldots\ldots\ldots\ldots\ldots\ldots\ldots\ldots\ldots\ldots\ldots\ldots\ldots\ldots\ldots\ldots (17)$$

Frequency factor of second order kinetics is obtained by the bellow the relation:

$$s = \frac{\beta E_a}{k_B T_M^2 \left(1 + \frac{2kT_M}{E_a}\right)} exp\left(\frac{E_a}{k_B T_M}\right) \quad \ldots\ldots\ldots\ldots\ldots\ldots\ldots\ldots\ldots\ldots\ldots\ldots\ldots\ldots\ldots\ldots\ldots\ldots\ldots\ldots\ldots\ldots\ldots\ldots\ldots\ldots (18)$$

Frequency factor of general order kinetics is obtained by the bellow the relation:

$$s = \frac{\beta E_a}{k_B T_M^2 \left[1 + \frac{2kT_M(b-1)}{E_a}\right]} exp\left(\frac{E_a}{k_B T_M}\right) \ldots\ldots\ldots\ldots\ldots\ldots\ldots\ldots\ldots\ldots\ldots\ldots (19)$$

where T_M is the maximum temperature for I_M, β is the heating rate (K/s), k is the Boltzmann's constant and E_a is the activation energy.

5.2.5. Instrumentation

The electronic functional block diagram of the TL reader conjugated with PC system and TL reader software shown in Figure 5.3. PC controlled TL reader type TL1009 manufactured by Nucleonix used for TL measurements of the phosphor is shown in Figure 5.4.

The TL reader consists of following segments of electronic circuits and other components.

***Low Voltage Supply*:** It is a DC power supply circuit that provide low voltage of the order of +5V @ 1A, +/- 12V @ 0.5A, +24V @0.5A. It provides power required for functionality of all the circuits. It consists an input line filter circuit, step down transformer with four secondary voltages, a three terminal regulator (bridge rectifier) and filter capacitors [81].

***High Voltage Module*:** High voltage power supply provides desire biasing voltage require to the photo multiplier tube because photo multiplier tube is negative biased to DC mode of operations in the voltage range of 0 to -1500V. The output of high voltage supply is a highly stabilized regulated voltage supply which generates (0-1500V) @ 1.0mA with less than 30mV rippled & noise (peak to peak).

***PMT bleeder circuit*:** The main work function of the photo multiplier tube (PMT) is to detect the light photon emitted during the heating process of phosphor that incident onto it, and to covert the light due to TL emission into D.C. current. PMT is biased by bleeder resistor network that operate it in low dark current mode. DC output of the PMT from the anode is applied to the I-F converter. For the DC current mode operation, the photo cathode of the PMT being connected to the negative bias and anode is connected with virtual zero potential [81].

***I/F (current to frequency) converter*:** A charge balancing type of current to frequency (I-F) converter circuit is used in TL reader. It has a linearity better than 1% over a frequency range from 1 Hz to 100 KHz. The work function of I-F circuit is to convert

anode current from the PMT into a continuous pulses of frequency proportional to the current [81].

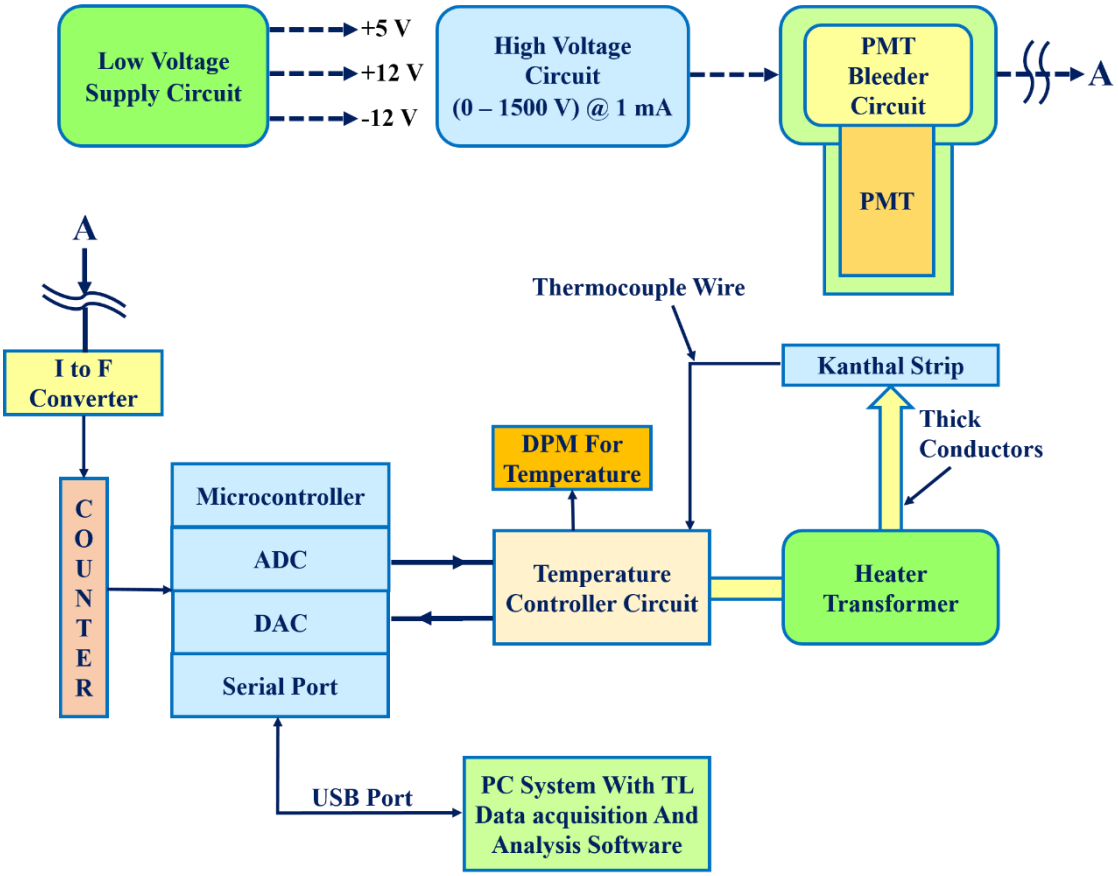

Figure 5.3 Block diagram of the TL Reader [81].

***Microcontroller with BCD counter, ADC, DAC, serial port*:** The work-functions of this section of the TL instrument are the temperature calibration data and interpret in terms of actual temperature, generate various heating profiles & heating rates, command instructions from the PC, to receive TTL pulses from I to F converter which corresponds to TL intensity data and storing them in the memory [82].

***Temperature controller*:** The temperature controller system is consists of heater transformer, heater element with thermocouple, millivolt amplifier, display modules (DPM). In this system, the thermocouple output of the order of millivolt received from the kanthal strip is fed to the monolithic thermo couple amplifier and the output from this is fed to an op-amp amplifier to appropriately condition the signal level. This signal is further fed to 3.5 digital DPM that can calibrated to indicate temperature of the kanthal strip. The signal consequently goes to ADC where the value of the signal is read by microcontroller that interpreted it in terms of temperature through PC program. Heater strip can be programmed to heat the sample from 1°C/sec up to 40°C/sec and a

max set temperature allowed is 500°C for various heating profile such as single or multiple plateaus [81, 82].

***Personal computer system* with *Data acquisition and analysis software*:** Personal computer (PC) system with TL instrument function software provides required graphical TL glow curve data acquisition and analysis software. The software perform following function: Heating profiles such as Linear, Single & Multi- plateau, Temperature Calibration, Light Stimulation Profile, Acquisition, Background spectrum / Sample data can be acquired, Background Subtraction, Export Spectrum data to Excel, Spectrum overlap, Spectrum subtraction [81, 82].

Figure 5.4 PC controlled TL reader type TL1009 manufactured by Nucleonix.

5.2.6. Applications

The TL phenomenon has been vastly studied by many researchers to understand the mechanism involved in thermally stimulated emission and it application in present. However, due to the deep knowledge of TL mechanism, the innovation and improvement in the TL instrumentation helped the researchers in various fields to solve their problems, out of large area of application some of the applications are explained briefly. Figure 5.5 shows some important applications of the TL phenomenon in present world are summarized in the chart.

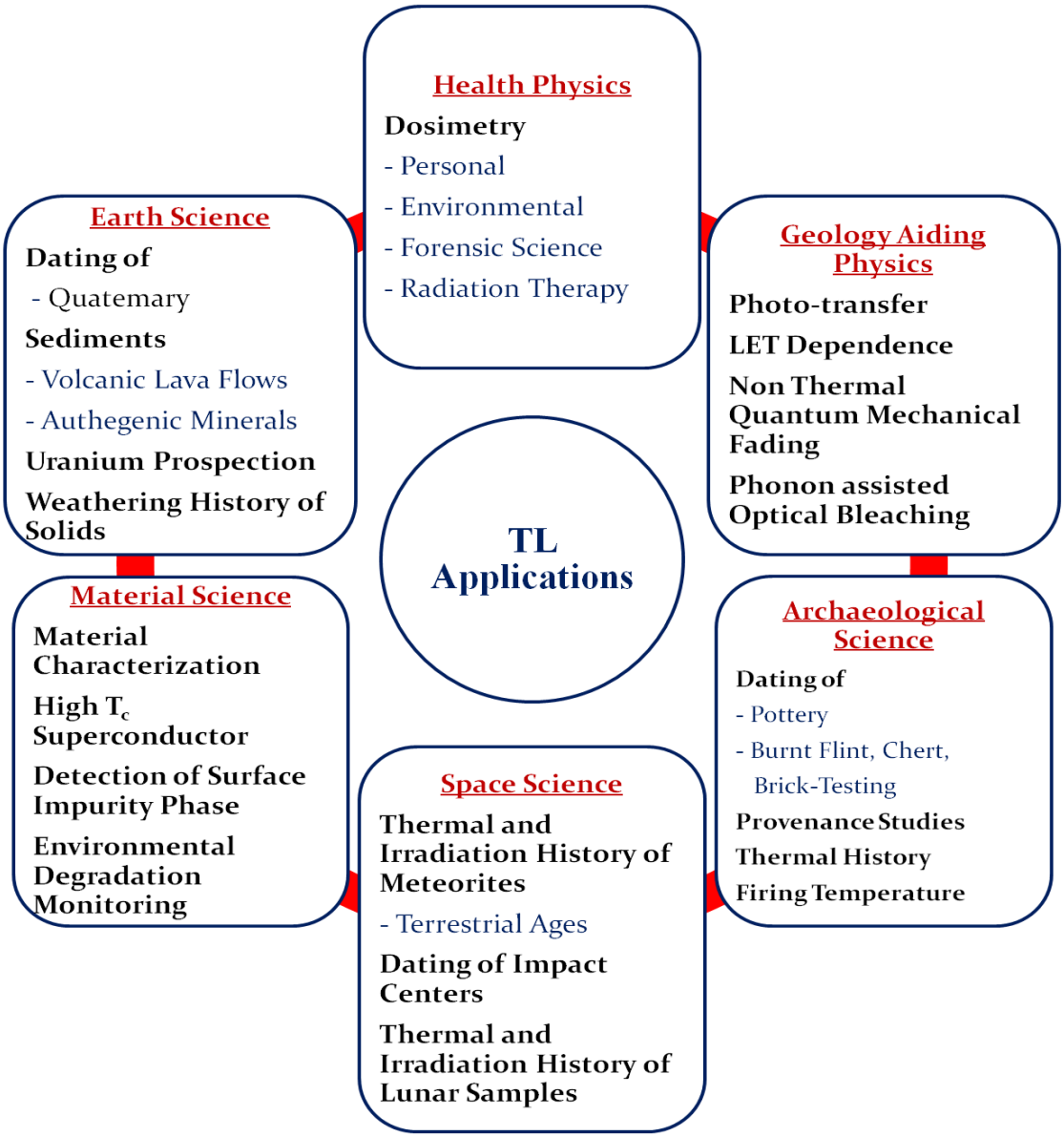

Figure. 5.5 Chart of applications of TL in different research disciplines.

5.2.6.1. TL Dosimetry (TLD)

Radiation dosimetry applications are the essential and fundamental requirement for the measurement of the ionization radiations and radioisotopes especially in Medical Physics and Science. Ionizing radiations mostly occurs at the places, where the X-rays, gamma radiation and beta particles mostly used for diagnosis and radiotherapy, X-rays are used in security system on airports and radiations emitted during the experimental studies in Physics and other Science braches. High-energy electrons, heavy particles and neutrons used in the major medical centers [83, 84].

TL dosimeter or TLD is a device used to measures the direct or indirect ionization radiation quantities like exposure, absorbed dose or equivalent dose, or their

time derivatives (rates). The selection of a phosphor for a TLD application needs a well-defined information of the specific application for what it is used to be under consideration. TLD applications are mainly bifurcate into three part that are the personal dosimetry for dose estimation of body tissue, environmental dosimetry for dose estimation in atmosphere, and medical dosimetry applications. The performance of a dosimeter is assessed by examining properties such as linearity, dose range, energy response, reproducibility, stability of stored information, isotropy, effect of environment on dosimeter performance, batch inhomogeneity, and others [29]. Several of these properties are now discussed in some detail before progressing to a discussion of individual phosphors.

Personnel Dosimetry

In personal dosimetry, the radiation dose measurement has been performed to measure the radiation absorbed by the personnel for the duration of their repetitive occupational exposure at working place. There are several working fields like nuclear industry, workers deal with X-ray units, hospital medical physicists, radiotherapy technicians, workers in industrial radiography, high intensity gamma irradiators and personnel on nuclear power plants, etc [85]. On the basis of monitoring such measurements of exposure, it is recognized that the personnel absorbed radiation under certain safety limits, which are prescribed by the International Commission of Radiological Protection (ICRP) for different field of application of radiation sources [86]. The most suitable TLD used for personnel dosimetry must have the desired characteristics such as tissue equivalent, Low fading, Accuracy (± 10% from 100 μGy to 10 Gy) [87].

Environmental Dosimetry

In recent years, the pollution due to the nuclear radiation causes critical problem in the health of living organism. The pollution mostly produce due to the gamma and UV radiation which is harmful dangerously for human being. Therefore the environmental regulatory authorities developed and under developed countries show more awareness about the environmental health [88]. In many countries the environmental monitoring has been done by TLD systems installed near the sources of nuclear radiation as well as the ionization radiation where it produces, such as nuclear power stations, low-level waste disposal, nuclear fuels reprocessing units, incidents of nuclear power station accidents places, nuclear power industry, etc [89, 90]. The phosphor used for the

environmental dosimetry is not require the tissue equivalence size. But the environment monitoring time is much longer so that the long exposure of material can take place. Therefore the TLD phosphor for environmental dosimetry should more stable and highly sensitive to the low radiation exposure [2, 28].

Medicinal Dosimetry

TLD material are widely used in medical science for the measurements of appropriate ionizing radiation dose given to patients during the diagnostic or therapy [83]. For that TLD exposed during the treatment are retrieved for analysing radiation dose, which can determine actual doses delivered to critical internal organs during these procedures and from such information are able to prescribe necessary additional treatments [91]. There are many departments where the clinical radiation are exposure to the humans such as x-ray exposure in mammography, dentistry and general health screening and radiotherapy [88]. The range of radiation dose use in radiology from 10^{-5} to 10^{-2} Gy, and up to 20-60 Gy in radiotherapy [85]. The TLD phosphors used in medical dosimetry tissue equivalency is the more important factor for the good TLD as well as the low radiation absorbance capacity of the phosphors.

5.2.6.2. Archaeological Science

Thermoluminescence (TL) technique is most powerful and efficient technique for the calculation of age of the ancient pottery since firing [44, 92]. The age of ancient pottery is determined as the time period for which it has been exposed to the irradiation following to its previous heating process. The TL dating of the ancient pottery is performed on the sensitive minerals like quartz situated in pottery or brick of the ancient structures by analysing the TL-output [93, 94]. The TL dating of pottery is very much similar to that the geological samples dating. The TL dating technique working on the fact that the crystalline materials have a capacity to store radiation energy derived from the radiations of radioactive substances contain in clay of pottery and cosmic radiation [95]. During the whole life, the pottery can absorb total natural radiations from internal radioactive substances such as alpha-, beta- and gamma-radiation as well as an external radiation from the cosmic rays which can be estimated using the dose rate data [44, 85]. Normally the materials from geological origin considerably absorb the radiation since their formation. But this stored energy is exhausted during the heating treatment of pottery at a fairly high temperature. At that time, the absorption event can reset the “TL clock” and only the energy stored since the

last date of such heating will be recorded [96]. Using a TL dating, it is possible to estimate the age of ancient pottery or archaeological object, if the rate of radiation energy stored in this materials can be measured and the formulation between the absorbed radiation and the emitted light is established. The relation for calculating the age of a specimen of pottery using TL is given bellow [97].

$$Age = \frac{Natural\ TL}{(TL\ per\ unit\ dose) \times (Natural\ dose\ rate)}$$

5.2.6.3. Geology

TL is one of the versatile technique to measure the geological age of the rocks. In nature the geological activities always take place for long period of time, in nature there are several radioactive elements exist in small amount inside the rock structure [98]. This types of rocks were exposed by the natural radiations emitted by radioactive elements. This rocks show natural thermoluminescence when they are heated. The thermoluminescence of rocks gives the information about the radiation accumulated in the rocks which give the information, how long this rocks were irradiated by such radiations and the age of rocks can be determined[99]. Thermoluminescence earliest used in Geology for variety of applications, such as dating of mineralization, igneous activities, sedimentation and evaluation of growth rate of beaches and sand dunes [85, 100]. Thermoluminescence technique is very useful for dating specimens of geologically recent origin.

5.3. Rare Earth Doped Strontium Pyrophosphate

Thermoluminescence study of the synthesized phosphor has been completed for the samples, xRE^{3+} (RE = Ce, Tb, Eu, Dy) doped $Sr_2P_2O_7$ for various concentration of dopant (x = 0.5, 1.0, 1.5, 2.0, 2.5, 5.0 mol%). Ce^{3+} and Dy^{3+} doped $Sr_2P_2O_7$ phosphors were prepared for the doping concentration 0.5 to 2.5 mol% of dopant. Eu^{3+} and Tb^{3+} doped $Sr_2P_2O_7$ phosphor were prepared for the doping concentration 0.5 to 5.0 mol% of dopant. All samples were firstly irradiated with irradiated by Sr^{90} β-source having decay rate 5 mCi for different time intervals for the doses of 0.048 to 0.48 Gy with accuracy of ±10%. The TL study were completed to investigate the dosimetry applications of synthesized phosphors. To achieve the purpose of application of the phosphors, TL characteristics of phosphor such as fading effect after exposure, linearity of TL output with doses, sensitivity for the reusability of phosphor were examined through the proper layout of experiments.

5.3.1. $Sr_2P_2O_7$: Ce^{3+}

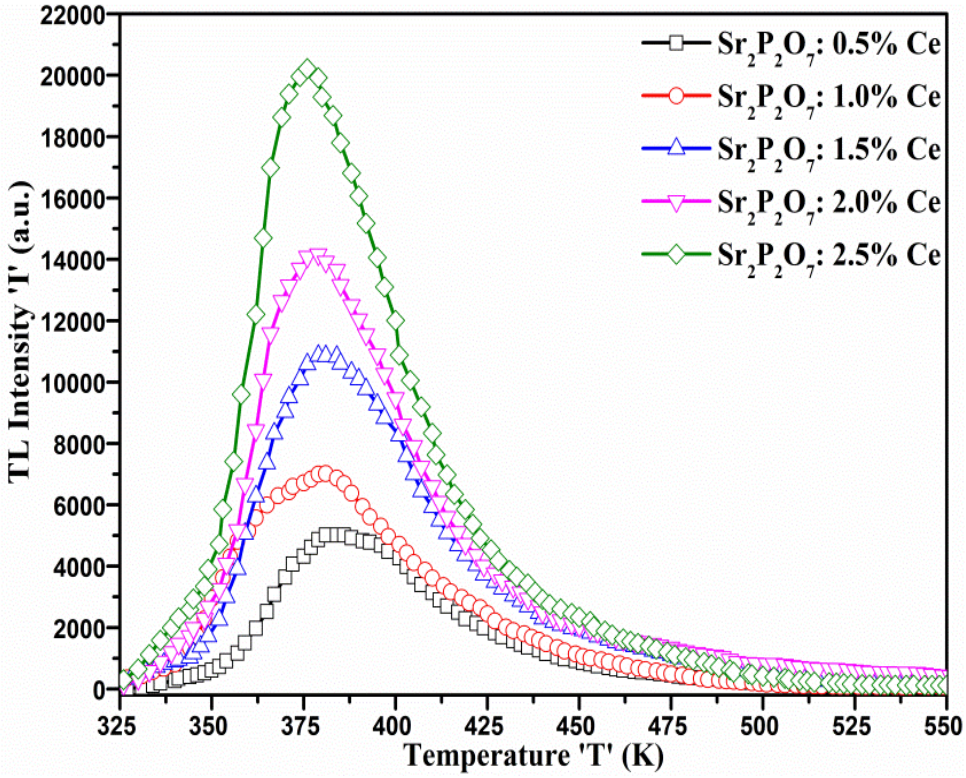

Figure 5.6 TL glow curve of $Sr_2P_2O_7$: x Ce^{3+} (x = 0.5, 1.0, 1.5, 2.0, 2.5 mol%) phosphors irradiated by β-radiation for 5 minute of 0.48 Gy dose.

Thermoluminescence (TL) properties of Ce^{3+} doped $Sr_2P_2O_7$ phosphors were studied by analysing TL output deviation on the basis of doping concentration, effect of irradiation time (Dose), linearity of TL intensity with amount of dose and fading effect in TL outcome with time, etc. For the study of TL properties, all the doped phosphors were irradiated by Sr^{90} β-source having decay rate 5 mCi for different time intervals 1, 2, 3, 4 and 5 minute. Figure 5.6 shows the TL glow curves of Ce^{3+} doped $Sr_2P_2O_7$ phosphor irradiated by β-radiation for 5 minute recorded for the temperature range 325 – 550 K. All glow curves were recorded for all Ce^{3+} doped phosphors in powder form at heating rate 6 K/s of the samples in fine powder form. Figure 5.7 shows the TL glow of Ce^{3+} doped $Sr_2P_2O_7$ carried out after β-irradiation of phosphors by 5 mCi Sr^{90} β-source for different irradiation time 1 to 5 minute, i.e., 0.097 to 0.48 Gy. The TL glow curves of Ce^{3+} doped $Sr_2P_2O_7$ phosphor exhibits prominent emission glow peak at 383 K temperature. The highest TL intensity is observed for the phosphor doped with 2.5 mol% Ce^{3+} and 5 minute radiation dose, which is for maximum concentration and maximum dose β-irradiation. The dose concentrations for different irradiation time

intervals are given in Table 5.1. The dose concentration has been calculated for 10 mg samples.

Irradiation Time 't'	Radiation Dose (D)
30 s	0.048 ± 0.005 Gy
1 minute	0.097 ± 0.01 Gy
2 minute	0.19 ± 0.02 Gy
3 minute	0.29 ± 0.03 Gy
4 minute	0.39 ± 0.04 Gy
5 minute	0.48 ± 0.05 Gy

Table 5.1 Radiation dose values for different irradiation time for β-radiation of Sr^{90}.

The TL glow curves is showing same kind of nature, i.e., uniform shape and structure for the different concentrations of Ce^{3+} doping. The TL outcomes of phosphor revealed that TL intensity of the glow curves increase linearly with doping concentration. The reason for increment in the TL intensity is the concentration of trapping center arises due to occupancy of Ce^{3+} increases within the host structure. TL study of Ce^{3+} of $Sr_2P_2O_7$ phosphor showed that doping of Ce^{3+} enhance the TL property of host. Because undoped $Sr_2P_2O_7$ phosphor showed poor TL properties due to the perfect crystal structure or may be due to low intrinsic defect, which cannot be useful for measure the absorbed dose. Doping of Ce^{3+} can be raise the trap centers in energy gap due to the incorporation of Ce^{3+} ions in host structure at Sr^{2+} site, which is steadily increases with doping concentration also identified in photoluminescence analysis, and resulting into the high TL performance.

Figure 5.8 shows the TL glow curve fitting of 2.5 mol% Ce^{3+} doped $Sr_2P_2O_7$ phosphor by GCD fitting method for general order kinetics. GCD fitting of the glow curve follows Kitis et al. equation of general order kinetics given by equation (15). TL glow curve has been fitted for fine value of figure of merit (FOM) 0.017% calculated by equation (16) using experimental and theoretically fitted TL glow curve. The GCD fitting of the glow curve revealed that the glow curve contain five peaks at different temperature with various peak intensity as mentioned in Table 5.3. These fine fitting represents that there could be five electron traps generated in the energy gap at different energy depth. The density of electron traps are increase at different energy level in energy gap due to the dose increment and increase in doping concentration of

Ce^{3+}[101]. This can be result into the reduction of broadening of TL glow curve with higher concentration and intensity increase rapidly. The analysis of fitted curve revealed that, the peak-I, Peak-II, peak-III, peak-IV and peak-V having order of kinetic 'b' values 1.8, 1.8, 2.0, 1.9 and 2.1 respectively, that follows the second order kinetics.

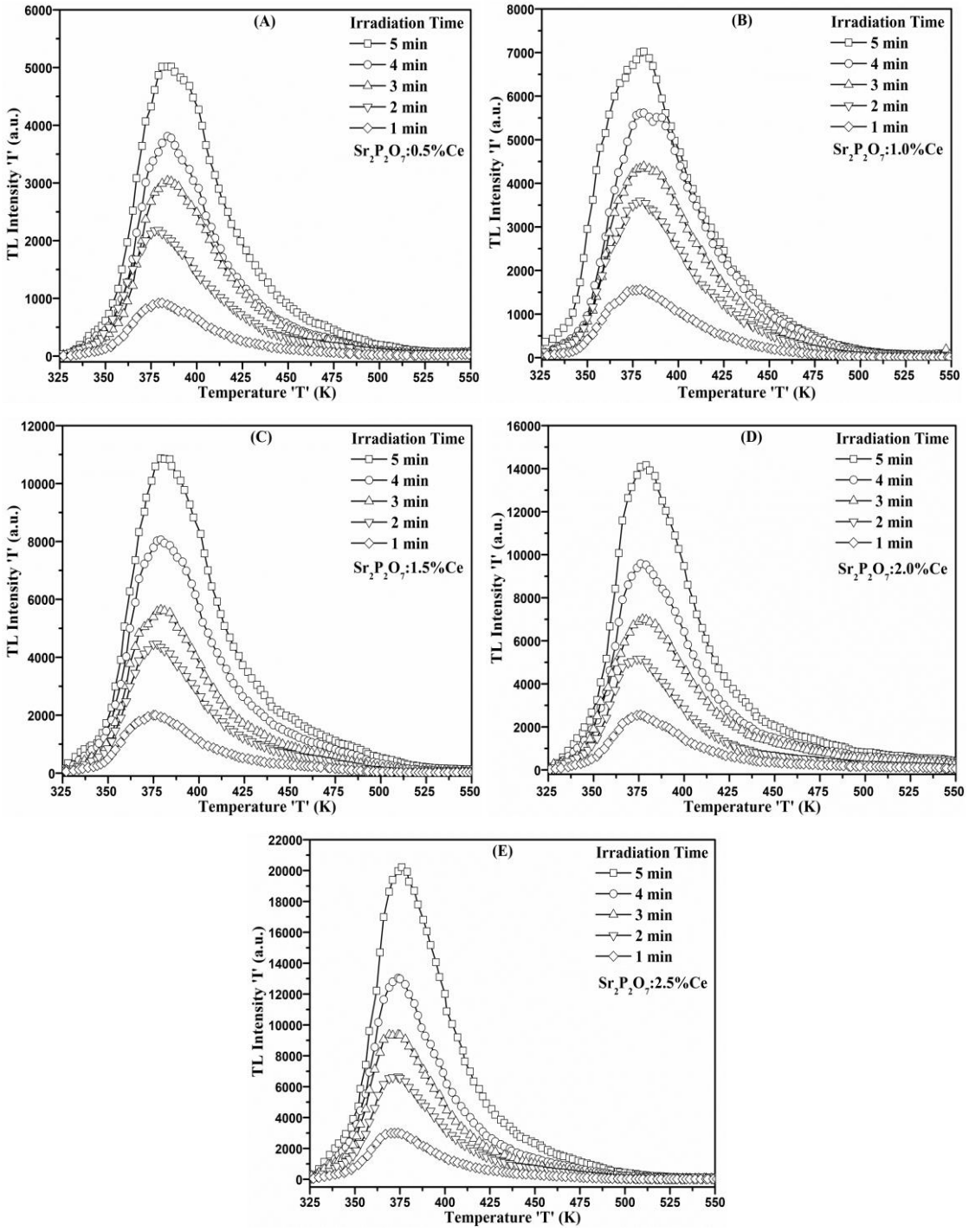

Figure 5.7 TL glow curves for various time of β-irradiation: (A) $Sr_2P_2O_7$: 0.5 mol% Ce^{3+}; (B) $Sr_2P_2O_7$: 1.0 mol% Ce^{3+}; (C) $Sr_2P_2O_7$: 1.5 mol% Ce^{3+}; (D) $Sr_2P_2O_7$: 2.0 mol% Ce^{3+}; (E) $Sr_2P_2O_7$: 2.5 mol% Ce^{3+}.

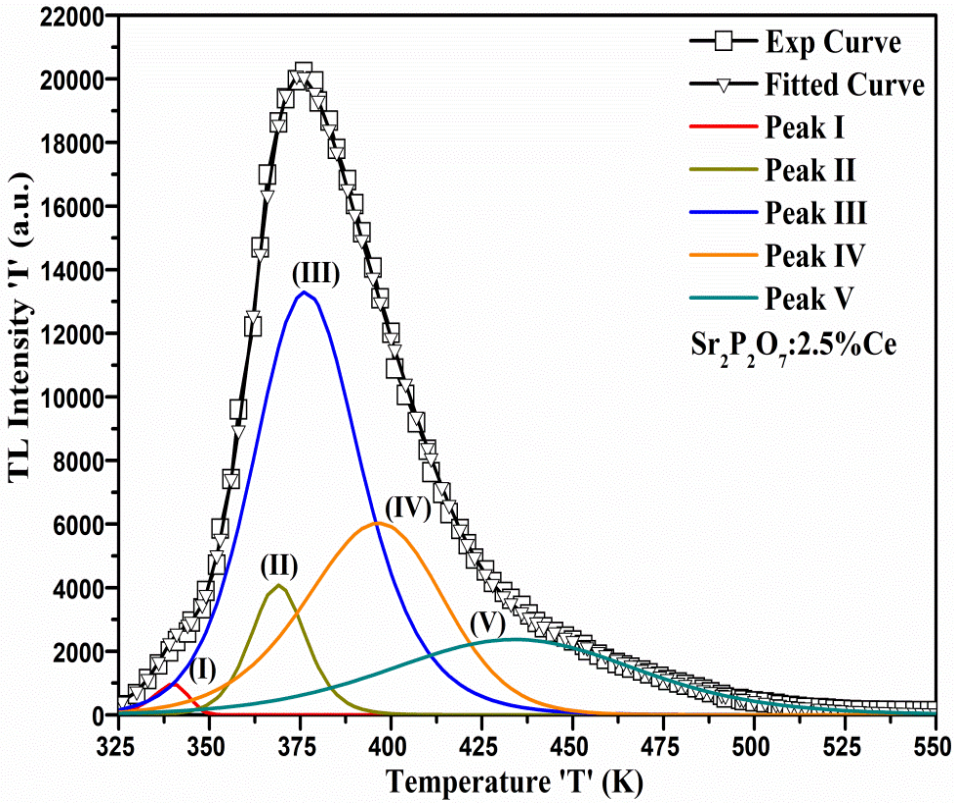

Figure 5.8 GCD fitting of TL glow curve of 2.5 mol% Ce^{3+} doped $Sr_2P_2O_7$ irradiated by β- radiation for 5 minute of 0.48 Gy dose.

The activation energy requires for trapping the electron from the trap centre is supplied to the phosphor by heating the sample. The calculated values of activation energy 'E_a' and the frequency factor 's' for different trap centre in 2.5 mol% Ce^{3+} doped $Sr_2P_2O_7$ phosphor were calculated through GCD method and are summarized in Table 5.2. Frequency factors 's' of each deconvoluted peaks were calculated from the equation (18) for second order kinetics. The activation energy 'E_a' of different peaks of 2.5 mol% Ce^{3+} doped $Sr_2P_2O_7$ phosphor are ranging from 2.41 to 0.57 eV. Frequency factor 's' are ranging 10^{11} to 10^{13} s^{-1} for different peaks. TL glow curve parameter also calculated by Chen's peak shape method (PSM) for second order kinetics. The activation energies involve in the glow curve formation of for 2.5 mol% Ce^{3+} doped $Sr_2P_2O_7$ phosphor are calculated by Chen's peak shape method (PSM). The formula for second order kinetics of PSM are given by equation (10), (11) and (12). TL parameters calculated by Chen's PSM is given in Table 5.3. The calculate values of geomantic factor 'μ_g' in PSM as mentioned in Table 5.3 are nearly equivalent to the value of second order kinetics. That suggests the PSM analysis is also truthful as GCD method [102].

Sample		Activation Energy 'Ea' (eV)	Order Of Kinetics 'b'	FOM %	Frequency Factor 's' (s^{-1})
$Sr_2P_2O_7$: 2.5 mol% Ce^{3+}	Peak I	2.37±0.06	1.8	0.017	1.17×10^{11}
	Peak II	2.15±0.06	1.8		2.23×10^{12}
	Peak III	1.17±0.05	2.0		7.54×10^{12}
	Peak IV	0.88±0.03	1.9		3.45×10^{13}
	Peak V	0.57±0.01	2.1		8.63×10^{13}

Table 5.2 Summary of TL kinetic parameters of glow curve for sample 2.5 mol% Ce^{3+} doped $Sr_2P_2O_7$ irradiated by β-radiation for 5 minute of 0.48 Gy dose calculated by GCD method.

Sample		I_{max}	T_{max} (K)	T_1 (K)	T_2 (K)	τ (K)	δ (K)	ω (K)	μ_g	Activation Energy		
										E_τ (eV)	E_δ (eV)	E_ω (eV)
$Sr_2P_2O_7$: 2.5 mol% Ce^{3+}	Peak I	949.3	339	333.5	345	5.5	6	11.5	0.522	2.41±0.06	2.45±0.04	2.43±0.05
	Peak II	4079.7	369	361.5	377	7.5	8	15.5	0.516	2.17±0.03	2.18±0.05	2.15±0.03
	Peak III	13295.1	376	359	394	17	18	35	0.514	1.15±0.04	1.13±0.03	1.16±0.02
	Peak IV	6028.2	395	373	418	22	23	45	0.511	0.92±0.02	0.87±0.02	0.90±0.01
	Peak V	2370.2	433	393	474	40	41	81	0.506	0.55±0.01	0.58±0.01	0.58±0.01

Table 5.3 Summary of TL kinetic parameters for 2.5 mol% Ce^{3+} doped $Sr_2P_2O_7$ irradiated by β-radiation for 5 minute of 0.48 Gy dose calculated by PSM.

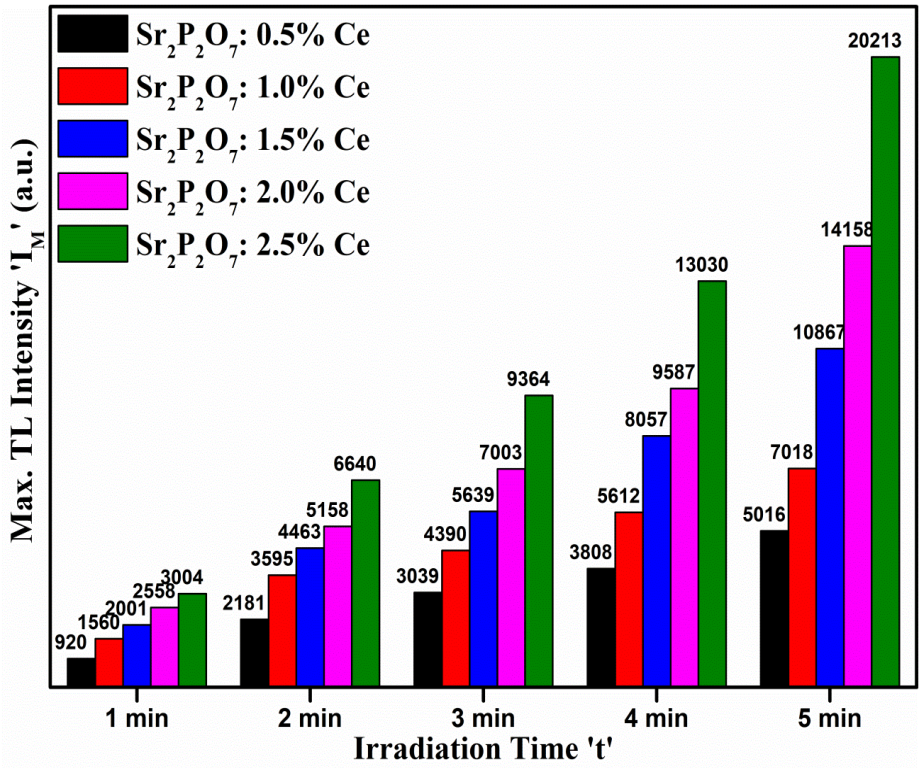

Figure 5.9 Maximum TL intensity 'I_M' vs β-irradiation time 't' graph of Ce^{3+} doped $Sr_2P_2O_7$.

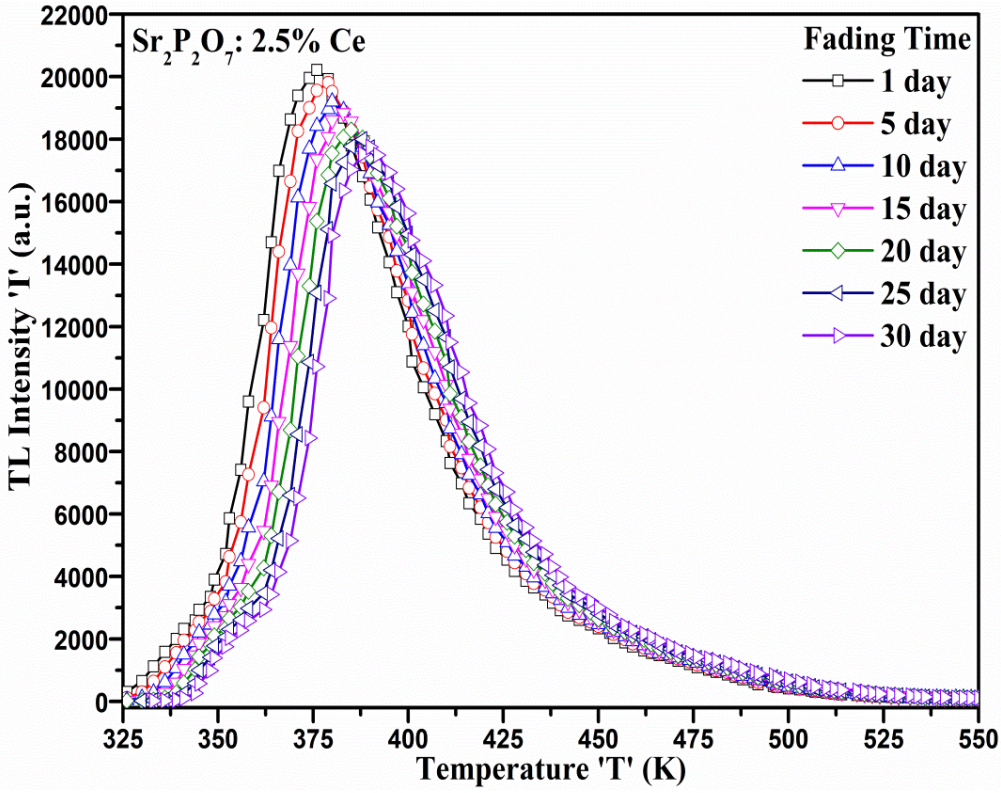

Figure 5.10 TL glow curve of $Sr_2P_2O_7$: 2.5 mol% Ce^{3+} phosphor irradiated by β-radiation for 5 minute of 0.48 Gy dose.

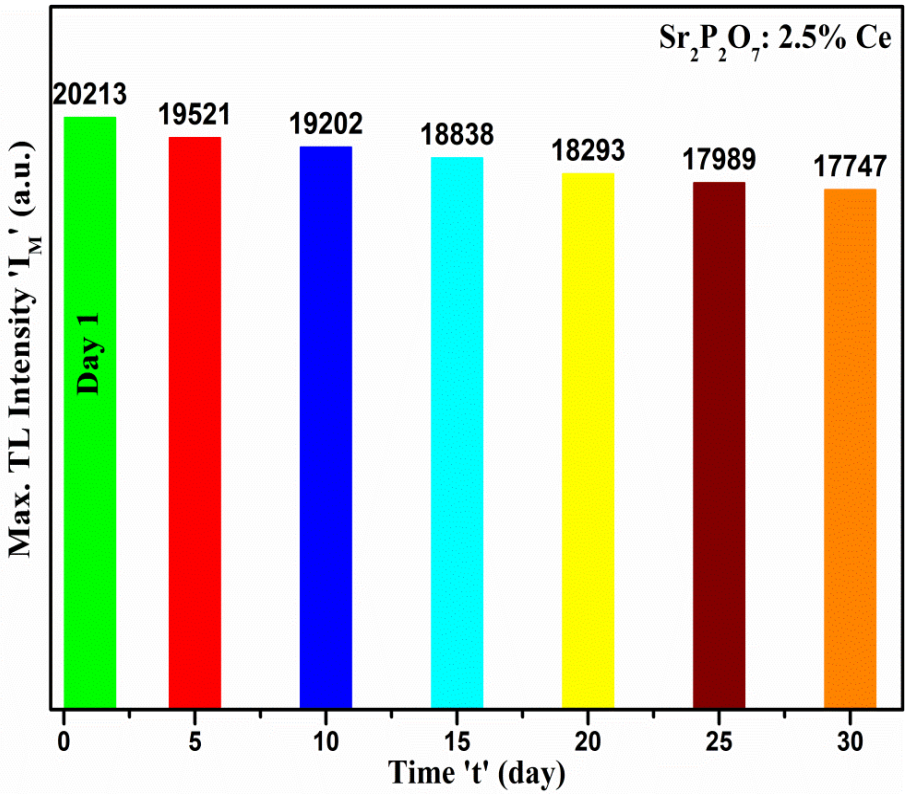

Figure 5.11 Maximum TL intensity 'I_M' vs Fading time 't' graph of $Sr_2P_2O_7$: 2.5 mol% Ce^{3+} phosphor irradiated by β-radiation for 5 minute of 0.48 Gy dose.

The phosphors used for dosimetry application have certain characteristic such as TL peak intensity of glow curve should be stable, the fading effect in TL peak should be zero or least after radiation exposure and reusability of phosphors. Figure 5.9 shows Maximum TL intensity (I_M) vs β-irradiation time 't' graph of Ce^{3+} doped $Sr_2P_2O_7$ for different concentrations of doping ion. The position of TL glow curve of the Ce^{3+} doped $Sr_2P_2O_7$ phosphor is stable for various dose exposure and various concentrations of doping. TL Intensity of Ce^{3+} doped $Sr_2P_2O_7$ phosphor vary linearly with amount radiation dose and doping concentration. The TL glow curves acquired to analyze the fading effect of TL glow curve for the period of one month at interval of five days for one month for all samples. The phosphors were stored in dark condition at room temperature after exposure of β-irradiation. Figure 5.10 shows TL glow curve of $Sr_2P_2O_7$: 2.5 mol% Ce^{3+} phosphor irradiated for 5 minute β- radiation to observed fading effect with time after exposure. The fading study of Ce^{3+} doped $Sr_2P_2O_7$ showed that the TL glow curve peak temperature shifted towards high temperature as the time elapsed, but the fading of peak maximum is much low about 2-3% per five days. Similar kind of fading effect were observed in all samples with different concentration

and doses. Figure 5.11 shows Maximum TL intensity (I_M) vs Fading time 't' graph of $Sr_2P_2O_7$: 2.5 mol% Ce^{3+} phosphor irradiated for 5 minute β- radiation.

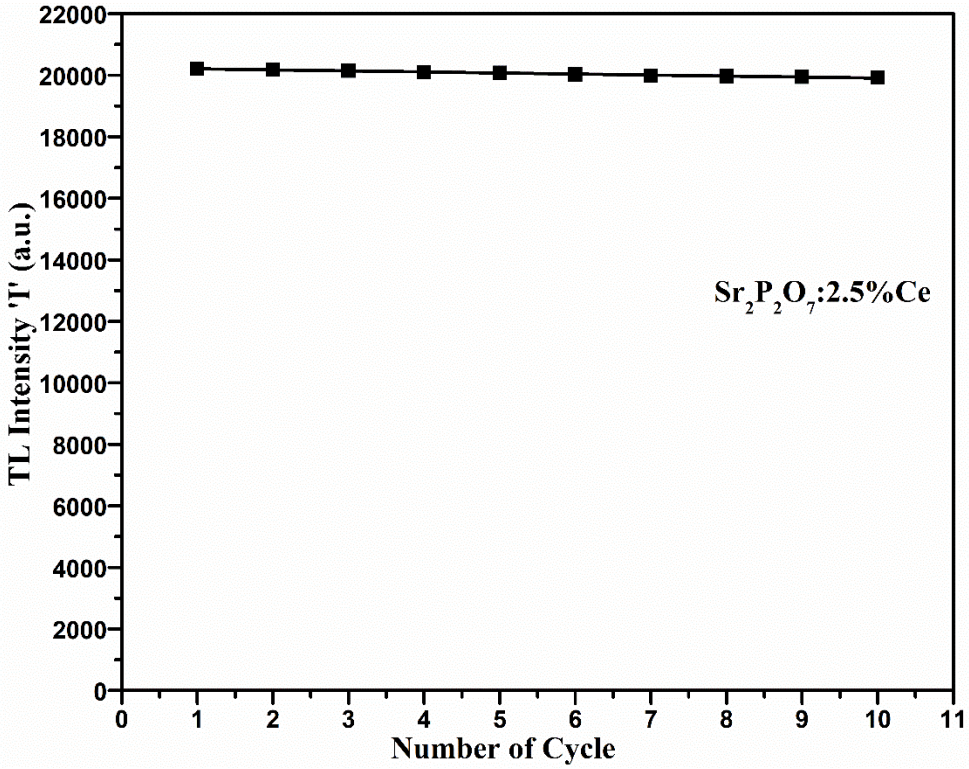

Figure 5.12 TL intensity vs Number of cycles of uses for $Sr_2P_2O_7$: 2.5 mol% Ce^{3+}.

The TL glow curve obtained from Ce^{3+} doped $Sr_2P_2O_7$ were consistent after long period of exposure of beta particles, that gives the information about the charge storage capacity of the $Sr_2P_2O_7$ phosphor. The sensitivity of TL phosphor was studied by observing the TL outcome of the phosphors by exposing the same phosphor for several time. That gives the significant result, where the TL intensity of the phosphor after repeated uses remains fractionally changed less than 7% of first to the tenth use of phosphor as shown in Figure 5.12 for $Sr_2P_2O_7$: 2.5 mol% Ce^{3+} phosphor. The result gives the significance of TL parameters like activation energy of traps remain unchanged after repeated readouts. Thus, Ce^{3+} doped $Sr_2P_2O_7$ can be considered as good phosphor for TLD application.

The analysis of glow curves revealed the significance of TL mechanism involve in glow curve formation. The activation energy, frequency factor and order of kinetics evaluated by both methods are very similar and consistent. The activation energy of different peak illustrates that the trap generated at different energy levels which require different excitation energy for detraping in holes. The measured values of trapping

parameters trough two different method are very similar that gives the significance of the TL outcome of Ce^{3+} doped $Sr_2P_2O_7$ phosphor.

5.3.2. $Sr_2P_2O_7$: Tb^{3+}

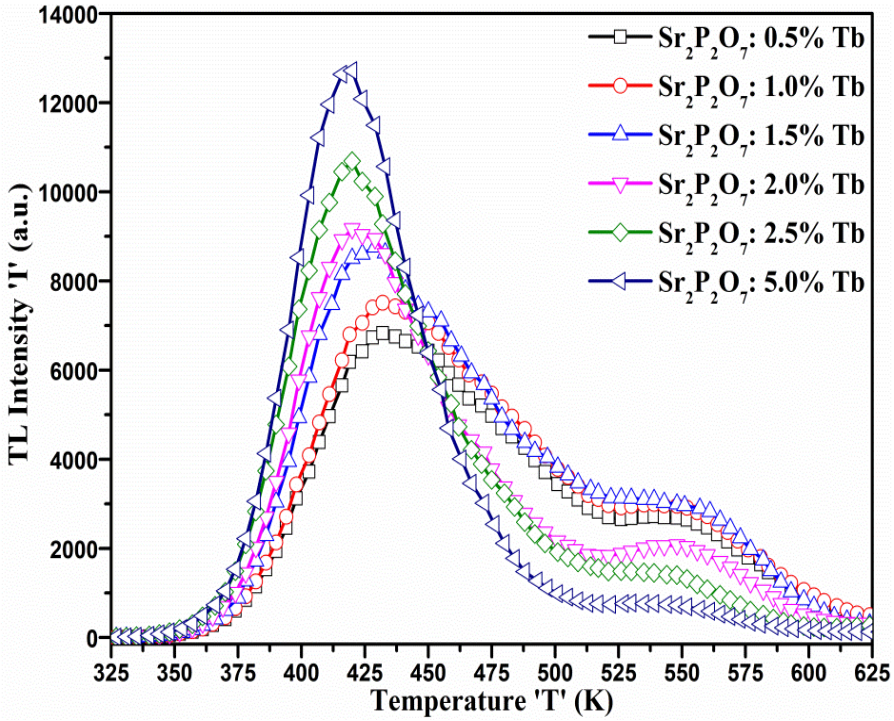

Figure 5.13 TL glow curve of $Sr_2P_2O_7$: x Tb^{3+} (x = 0.5, 1.0, 1.5, 2.0, 2.5, 5.0 mol%) phosphors irradiated by β-radiation for 5 minute of 0.48 Gy dose.

Figure 5.13 shows the TL glow curves of Tb^{3+} doped $Sr_2P_2O_7$ phosphor irradiated by β- radiation for 5 minute. The TL glow curves were recorded for the temperature range 325 – 625 K at heating rate 6 K/s for different doping concentrations. Glow curves consists of prominent glow peak at around 434 K and shoulder peak at around 550 K temperature. Thermoluminescence (TL) properties of Tb^{3+} doped $Sr_2P_2O_7$ phosphor was studied by analysing TL output deviation on the basis of doping concentration, effect of irradiation time (Dose), linearity of TL intensity with dose concentration and fading effect in TL outcome with time, etc. For the study of TL properties, all the doped phosphors were irradiated by Sr^{90} β-source having decay rate 5 mCi for different time intervals 30 s, 1, 2, 3, 4 and 5 min, i.e., 0.048 to 0.48 Gy. Figure 5.14 shows the TL glow curves of Tb^{3+} doped $Sr_2P_2O_7$ phosphor irradiated by β-radiation for different time interval of radiation exposure. From the TL glow curve, it is noted that the TL intensity increases as the time interval of irradiation increases, i.e., dose of exposure.

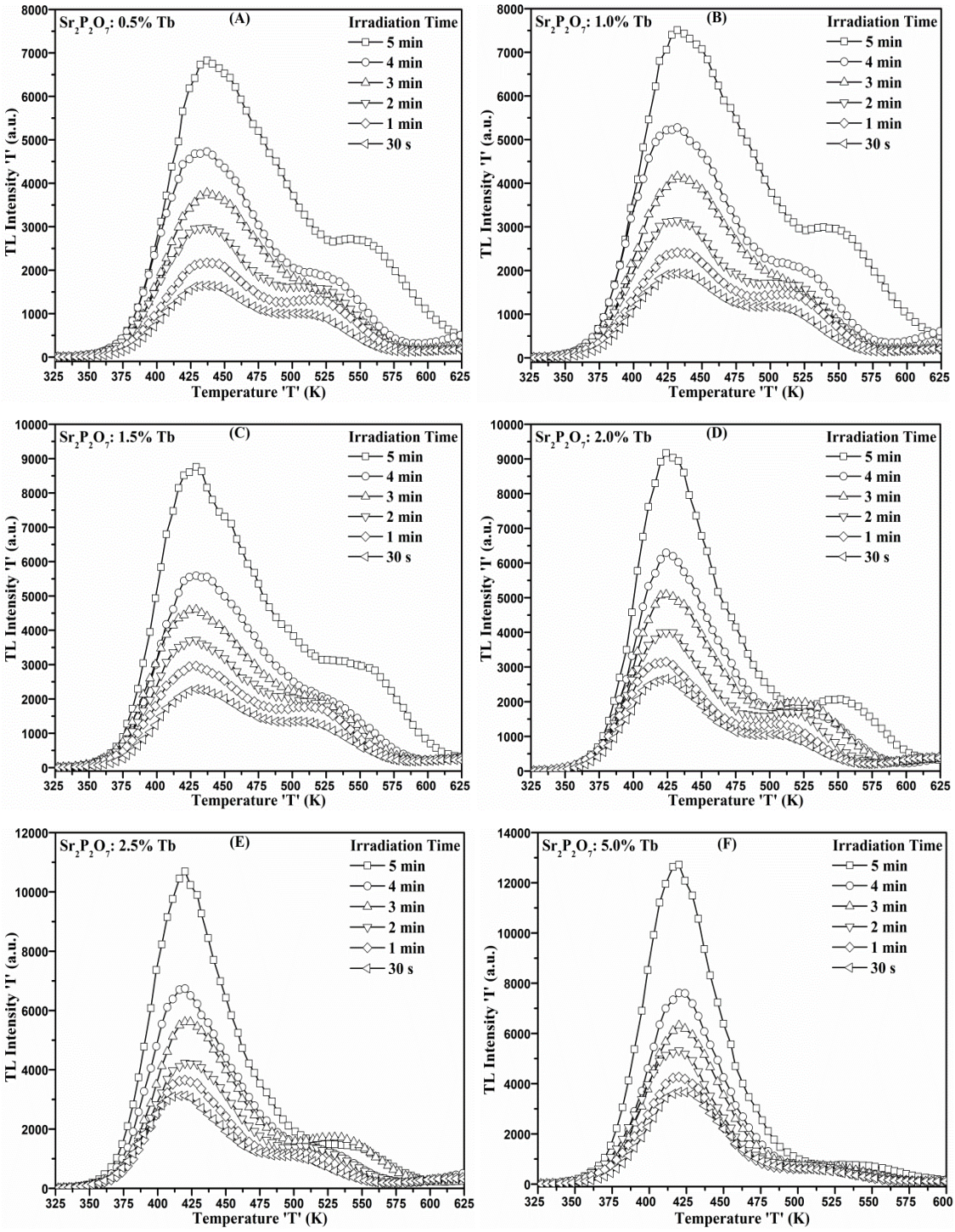

Figure 5.14 TL glow curve for various time of β-irradiation: (A) $Sr_2P_2O_7$: 0.5 mol% Tb^{3+}; (B) $Sr_2P_2O_7$: 1.0 mol% Tb^{3+}; (C) $Sr_2P_2O_7$: 1.5 mol% Tb^{3+}; (D) $Sr_2P_2O_7$: 2.0 mol% Tb^{3+}; (E) $Sr_2P_2O_7$: 2.5 mol% Tb^{3+}; (F) $Sr_2P_2O_7$: 5.0 mol% Tb^{3+}.

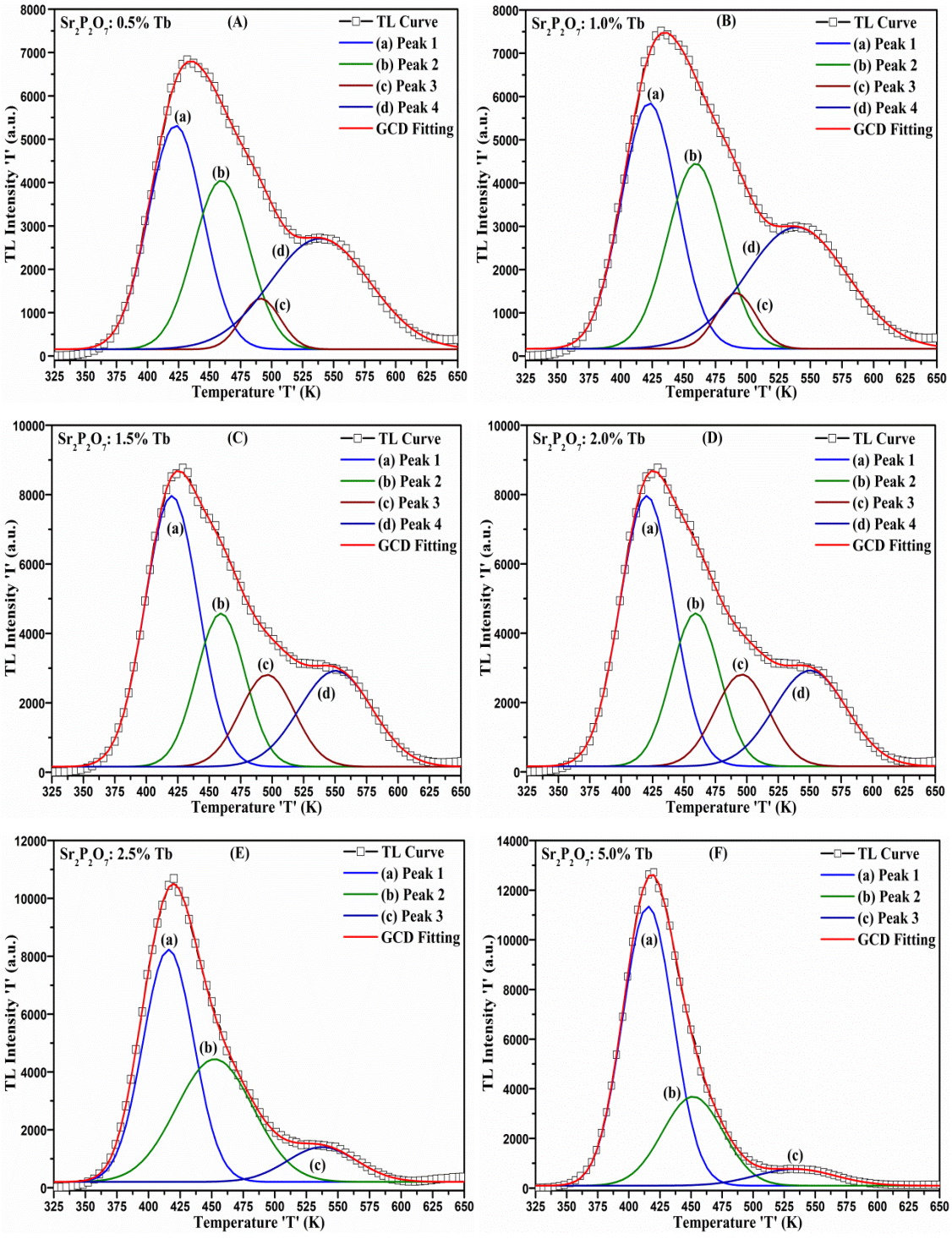

Figure 5.15 GCD fitting of TL glow curves of (A) $Sr_2P_2O_7$: 0.5 mol% Tb^{3+}; (B) $Sr_2P_2O_7$: 1.0 mol% Tb^{3+}; (C) $Sr_2P_2O_7$: 1.5 mol% Tb^{3+}; (D) $Sr_2P_2O_7$: 2.0 mol% Tb^{3+}; (E) $Sr_2P_2O_7$: 2.5 mol% Tb^{3+}; (F) $Sr_2P_2O_7$: 5.0 mol% Tb^{3+}.

From Figure 5.14, it is also noted that the TL intensity increases with increase in doping concentration of Tb^{3+} ion. Figure 5.14 shows that the shape of glow curve changes with doping concentration, where the second peak intensity at higher

temperature 562 K is decreasing gradually with higher concentration and all most weakened for the doping concentration of 5 mol% of Tb^{3+}. As the radiation dose increase the second peak position move towards the higher temperature that could be observed due to the variation of trap depth with dose amount. The higher dose of radiation can change the trap depth and density of the electron trap [103].

TL parameters of glow of glow such as activation energy, frequency factor, order of kinetics involve in TL mechanism have been calculated by two different methods. Figure 5.15 shows the GCD fitting of TL glows of Tb^{3+} doped $Sr_2P_2O_7$ phosphor recorded after 5 minute β- radiation. GCD fitting of the glow curves have been done through the Kitis et al. equation of general order kinetics given by equation (15). TL glow curves have been fitted for fine value of figure of merit (FOM) calculated by equation (16) using experimental and theoretically fitted TL glow curves. Figure of merit (FOM) for different fitted curve are mentioned in Table 5.4, which is small for the fine fitting curves. The GCD fitting of the glow curve revealed that the glow curves of 0.5 – 2.0 mol% Tb^{3+} consists of four peaks while the glow curves of 2.5 and 5.0 mol% Tb^{3+} consists of three peaks located at different temperature with various peak intensity as mentioned in Table 5.5. The fine GCD fitting revealed that there are four trap levels involved in 0.5 – 2.0 mol% Tb^{3+} and three trap levels involved in 5.5 – 5.0 mol% Tb^{3+}, that are developed in the energy gap at different energy depth due to Tb^{3+} doping. As observed in Ce^{3+} doped phosphors, the electron traps are increase at different trapping level in energy gap due to the dose increment and increase in doping concentration, which results into the intensity increases and reduction of broadening of TL glow curve with higher concentration occurs accordingly. The GCD analysis of all fitted glow curves revealed that the peak-I, Peak-II, peak-III and peak-IV follow the second order kinetics. The values of order of kinetics 'b' are 1.9, 1.8, 1.8, and 2.1 for peak I, II, III, and IV for the samples having doping concentration level 0.5 – 2.0 mol% of Tb^{3+}, and 1.9, 1.8, 2.1 for peak I, II, and III for the samples having doping concentration level 2.5 – 5.0 mol% of Tb^{3+}. The order of kinetics 'b' value for different peaks are summarized in Table 5.4. The activation energy 'E_a' for electron traps are ranging from 0.82 to 1.52 eV and frequency factor 's' are ranging from 10^{11} to 10^{13} s^{-1}. The corresponding values of activation energy 'E_a' and frequency factor 's' for different trap centre in Tb^{3+} doped $Sr_2P_2O_7$ phosphor obtained through GCD method are summarized in Table 5.4.

Sample		Activation Energy 'E$_a$' (eV)	Order Of Kinetics 'b'	FOM %	Frequency Factor 's' (s^{-1})
$Sr_2P_2O_7$: 0.5 mol% Tb^{3+}	Peak I	0.93±0.04	1.9	0.25	2.39×10^{11}
	Peak II	1.01±0.04	1.8		4.25×10^{11}
	Peak III	1.50±0.08	1.8		5.56×10^{13}
	Peak IV	0.83±0.03	2.1		1.26×10^{12}
$Sr_2P_2O_7$: 1.0 mol% Tb^{3+}	Peak I	0.82±0.03	1.9	0.21	2.57×10^{11}
	Peak II	1.02±0.05	1.8		4.43×10^{11}
	Peak III	1.52±0.06	1.8		5.28×10^{13}
	Peak IV	0.76±0.02	2.1		1.45×10^{12}
$Sr_2P_2O_7$: 1.5 mol% Tb^{3+}	Peak I	0.97±0.03	1.9	0.18	2.11×10^{11}
	Peak II	1.19±0.05	1.8		4.59×10^{11}
	Peak III	1.21±0.04	1.8		5.64×10^{13}
	Peak IV	1.15±0.03	2.1		2.05×10^{12}
$Sr_2P_2O_7$: 2.0 mol% Tb^{3+}	Peak I	0.93±0.03	1.9	0.13	2.37×10^{11}
	Peak II	1.19±0.06	1.8		4.78×10^{11}
	Peak III	1.08±0.04	1.8		5.75×10^{13}
	Peak IV	1.10±0.04	2.1		2.35×10^{12}
$Sr_2P_2O_7$: 2.5 mol% Tb^{3+}	Peak I	1.00±0.05	1.9	0.12	2.46×10^{11}
	Peak II	0.83±0.02	1.8		4.89×10^{11}
	Peak III	1.11±0.05	2.1		2.67×10^{12}
$Sr_2P_2O_7$: 5.0 mol% Tb^{3+}	Peak I	0.95±0.03	1.9	0.09	2.29×10^{11}
	Peak II	0.86±0.03	1.8		2.54×10^{11}
	Peak III	0.91±0.03	2.1		2.55×10^{12}

Table 5.4 Summary of TL kinetic parameters of glow curve for sample Tb^{3+} doped $Sr_2P_2O_7$ irradiated by β-radiation for 5 minute of 0.48 Gy dose calculated by GCD method.

Sample		I_{max}	T_{max} (K)	T_1 (K)	T_2 (K)	τ (K)	δ (K)	ω (K)	μ_g	Activation Energy		
										E_τ (eV)	E_δ (eV)	E_ω (eV)
$Sr_2P_2O_7$: 0.5 mol% Tb^{3+}	Peak I	5309.63	424	396	450	28	25.5	53.5	0.48	0.81±0.04	0.90±0.03	0.86±0.02
	Peak II	4039.64	458	433	486	25	28	53	0.52	1.09±0.04	0.96±0.04	1.02±0.02
	Peak III	1325.89	492	471	512	21	20	41	0.49	1.55±0.08	1.55±0.08	1.56±0.04
	Peak IV	2709.81	539	490	589	49	50	99	0.51	0.70±0.02	0.74±0.01	0.72±0.01
$Sr_2P_2O_7$: 1.0 mol% Tb^{3+}	Peak I	5841.15	424	397	449	27	25	52	0.48	0.85±0.05	0.92±0.04	0.89±0.03
	Peak II	4443.09	458	432	487	26	29	55	0.52	1.05±0.04	0.93±0.05	0.98±0.04
	Peak III	1459.03	492	471	511	21	19	40	0.47	1.55±0.07	1.63±0.06	1.60±0.08
	Peak IV	2980.80	539	489	590	50	51	101	0.50	0.69±0.01	0.73±0.02	0.71±0.01
$Sr_2P_2O_7$: 1.5 mol% Tb^{3+}	Peak I	7965.38	420	395	445	25	25	50	0.50	0.91±0.03	0.90±0.02	0.91±0.03
	Peak II	4577.37	459	436	481	23	22	45	0.49	1.21±0.05	1.23±0.07	1.22±0.04
	Peak III	2808.61	497	469	523	28	26	54	0.48	1.14±0.06	1.22±0.05	1.19±0.06
	Peak IV	2925.76	551	515	586	36	35	71	0.49	1.07±0.02	1.11±0.03	1.09±0.03
$Sr_2P_2O_7$: 2.0 mol% Tb^{3+}	Peak I	7843.32	421	396	445	25	24	49	0.49	0.91±0.03	0.95±0.02	0.93±0.04
	Peak II	4489.23	458	437	481	21	23	44	0.52	1.33±0.06	1.17±0.08	1.25±0.06
	Peak III	2746.45	496	470	524	26	28	54	0.52	1.24±0.04	1.12±0.05	1.18±0.05
	Peak IV	2896.23	552	514	588	38	36	74	0.49	1.01±0.03	1.08±0.04	1.05±0.03
$Sr_2P_2O_7$: 2.5 mol% Tb^{3+}	Peak I	8236.39	416	391	439	25	23	48	0.48	0.89±0.03	0.96±0.04	0.93±0.04
	Peak II	4436.41	452	415	490	39	36	75	0.50	0.78±0.01	0.79±0.02	0.79±0.02
	Peak III	1402.27	539	502	573	37	34	71	0.48	0.99±0.05	1.09±0.07	1.05±0.06
$Sr_2P_2O_7$: 5.0 mol% Tb^{3+}	Peak I	11342.8	416	392	440	24	24	48	0.50	0.93±0.04	0.92±0.04	0.93±0.03
	Peak II	3677.39	450	422	481	28	31	59	0.52	0.93±0.03	0.84±0.03	0.88±0.04
	Peak III	766.36	535	492	576	43	41	84	0.49	0.81±0.03	0.89±0.02	0.86±0.05

Table 5.5 Summary of TL kinetic parameters for Tb^{3+} doped $Sr_2P_2O_7$ irradiated by β-radiation for 5 minute of 0.48 Gy dose calculated by PSM.

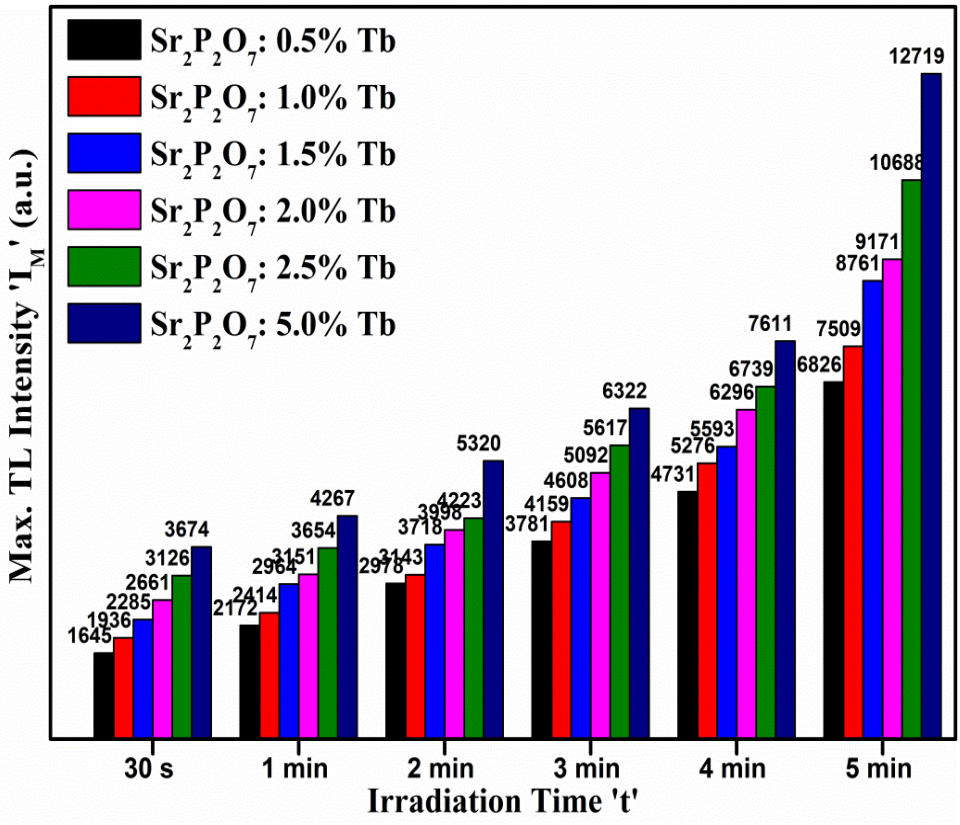

Figure 5.16 Maximum TL intensity 'I_M' vs β-irradiation time 't' graph of Tb^{3+} doped $Sr_2P_2O_7$.

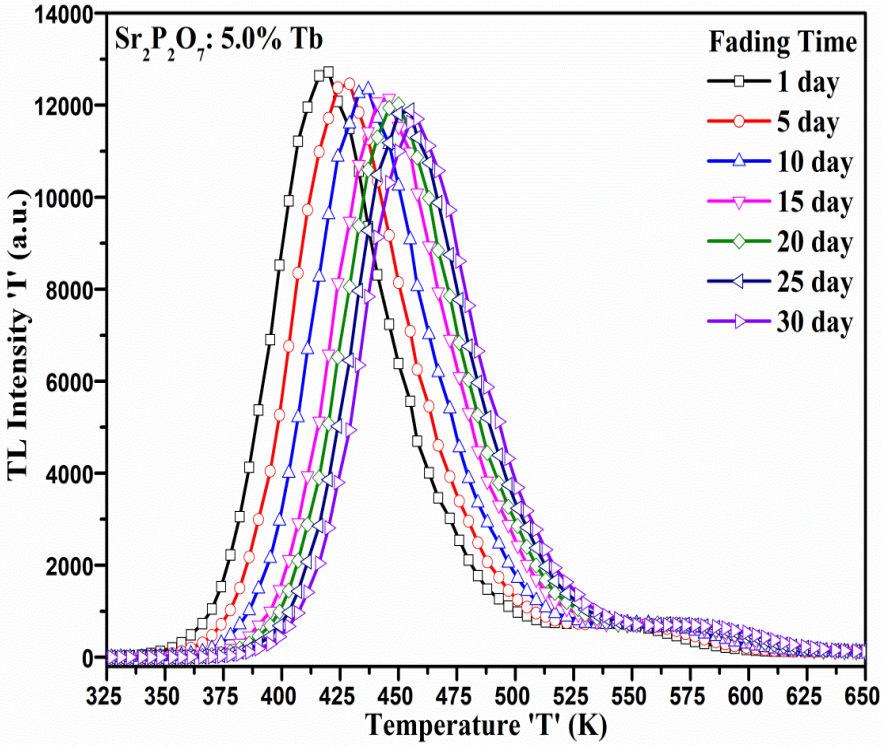

Figure 5.17 TL glow curve of $Sr_2P_2O_7$: 5.0 mol% Tb^{3+} phosphor irradiated by β-radiation for 5 minute of 0.48 Gy dose.

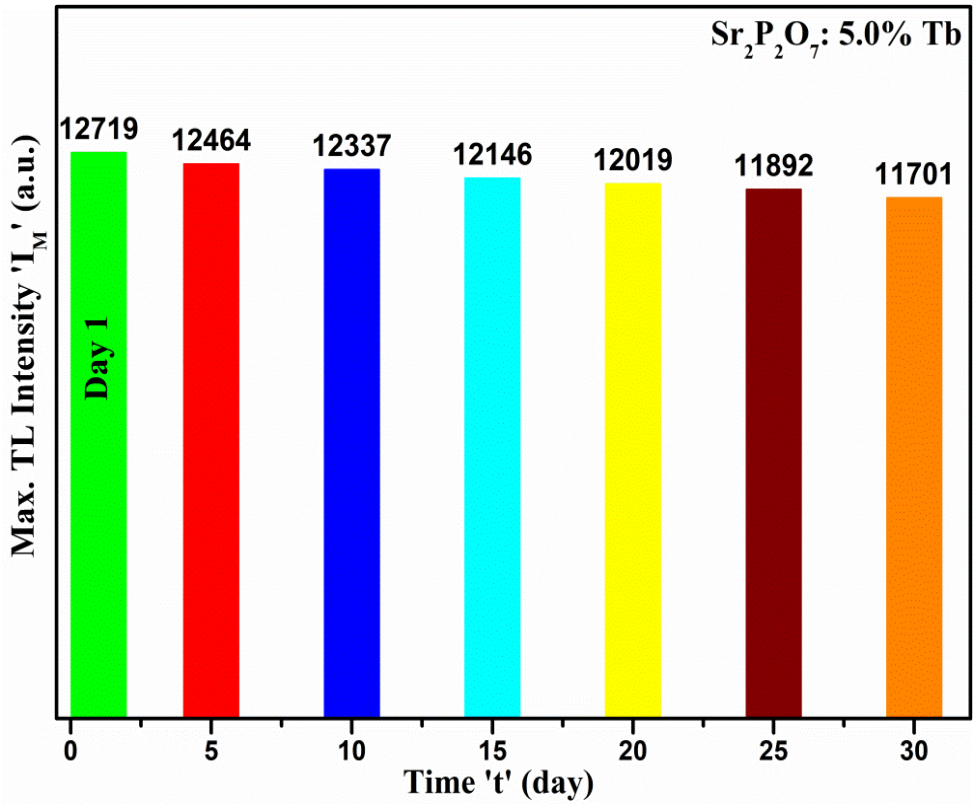

Figure 5.18 Maximum TL intensity 'I_M' vs Fading time 't' graph of 5.0 mo% Tb^{3+} doped $Sr_2P_2O_7$ irradiated by β-radiation for 5 minute of 0.48 Gy dose.

The TL glow curve parameter also calculated by Chen's peak shape method (PSM) for second order kinetics given by equation (10), (11) and (12). The activation energy of each glow curve calculated from PSM were nearer to the values obtained by GCD method. TL parameters calculated by Chen's PSM method for all Tb^{3+} doped $Sr_2P_2O_7$ phosphors are given in Table 5.5. The values of geometric factor 'μ_g' are similar that of the second order kinetics that is nearby 0.52, which suggests the glow curves follow second order kinetics that derived in GCD method.

Figure 5.16 shows Maximum TL intensity vs β-irradiation time graph of Tb^{3+} doped $Sr_2P_2O_7$ for different concentrations of doping ion. To examine the effect of various doses, the TL response of the phosphors have been observed after exposing at different β-radiation doses. TL response after different doses and doping concentration relation shows linear relation, i.e., the TL intensity increases gradually with both the way. Figure 5.17 shows TL glow curve of $Sr_2P_2O_7$: 5.0 mol% Tb^{3+} phosphor irradiated by irradiated by β- radiation for 5 minute to observed fading effect with time after exposure. The TL glow curves were acquired to analyze the fading effect of TL glow curve for one month at interval of five days for one month for all samples. The

phosphors were stored in dark condition at room temperature after exposure of β-radiation. This fading study showed that the TL glow curve peak temperature 420 K is shifted towards higher temperature as the time elapsed, but the fading of peak maximum is much small. The fading rate of TL intensity is 2-3% per 5 days. Similar kind of fading effect were observed in all samples with different concentration and doses. Figure 5.18 shows Maximum TL intensity vs Fading time graph of $Sr_2P_2O_7$: 5.0 mol% Tb^{3+} phosphor irradiated by β- radiation for 5 minute.

5.3.3. $Sr_2P_2O_7$: Eu^{3+}

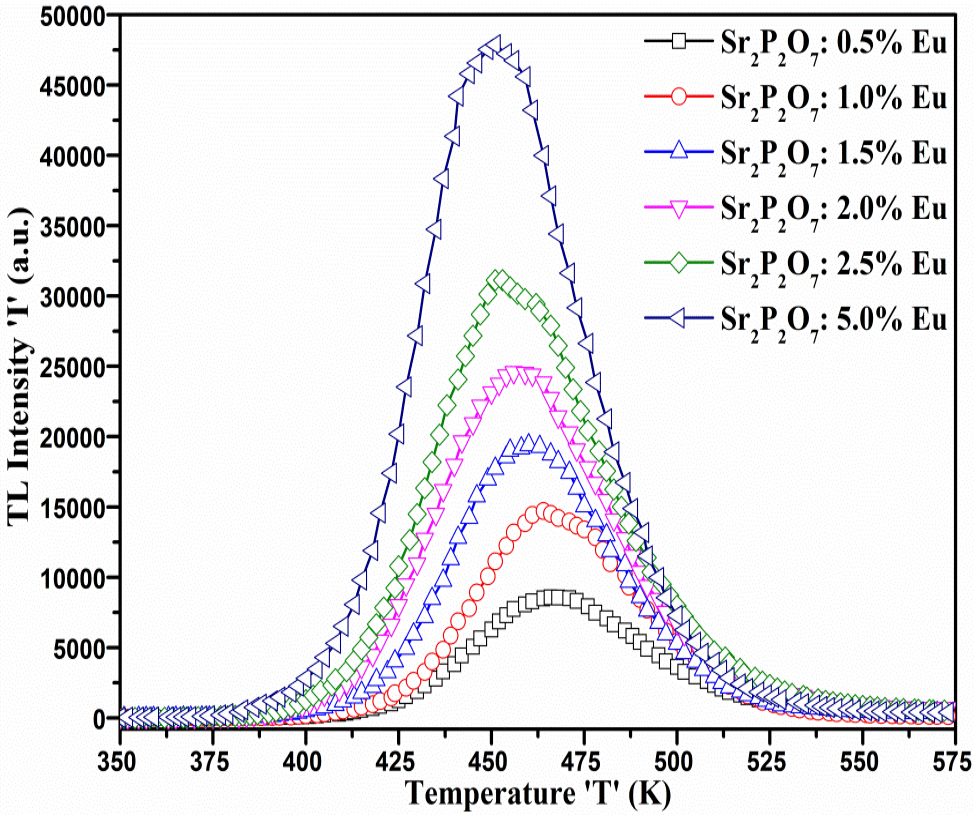

Figure 5.19 TL glow curve of $Sr_2P_2O_7$: x Eu^{3+} (x = 0.5, 1.0, 1.5, 2.0, 2.5, 5.0 mol%) phosphors irradiated by β-radiation for 5 minute of 0.48 Gy dose.

In general observation TL study, it is found that the TL intensity of phosphor is significantly depends on the doping concentration and the radiation dose absorbed by phosphors. Figure 5.19 shows the TL glow curves of Eu^{3+} doped $Sr_2P_2O_7$ irradiated by β-radiation for 5 min. It shows the TL glow curve intensity increases as the concentration of doping increases, while the peak position shifting toward the higher temperature for lower concentration. TL glow curves of Eu^{3+} doped $Sr_2P_2O_7$ phosphor consists of single bell shape curves. The highest intensity exhibits at 452 K temperature

for 5.0 mol% Eu^{3+} doped $Sr_2P_2O_7$ and 467 K for 0.5 mol% Eu^{3+} doped $Sr_2P_2O_7$ which signify that the position of electron trap cent are changes with doping concentration.

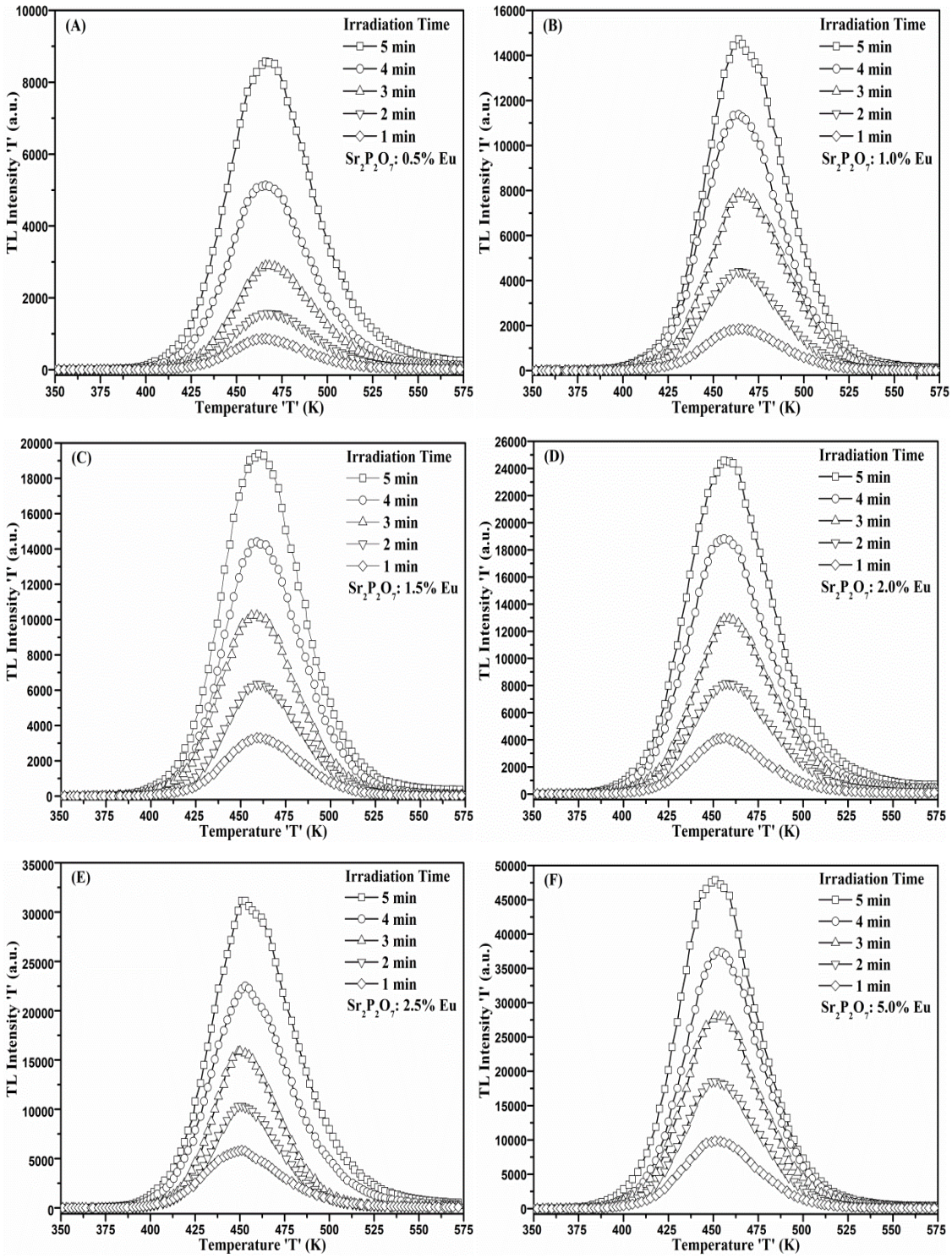

Figure 5.20 TL glow curve for various time of β-irradiation: (A) $Sr_2P_2O_7$: 0.5 mol% Eu^{3+}; (B) $Sr_2P_2O_7$: 1.0 mol% Eu^{3+}; (C) $Sr_2P_2O_7$: 1.5 mol% Eu^{3+}; (D) $Sr_2P_2O_7$: 2.0 mol% Eu^{3+}; (E) $Sr_2P_2O_7$: 2.5 mol% Eu^{3+}; (F) $Sr_2P_2O_7$: 5.0 mol% Eu^{3+}.

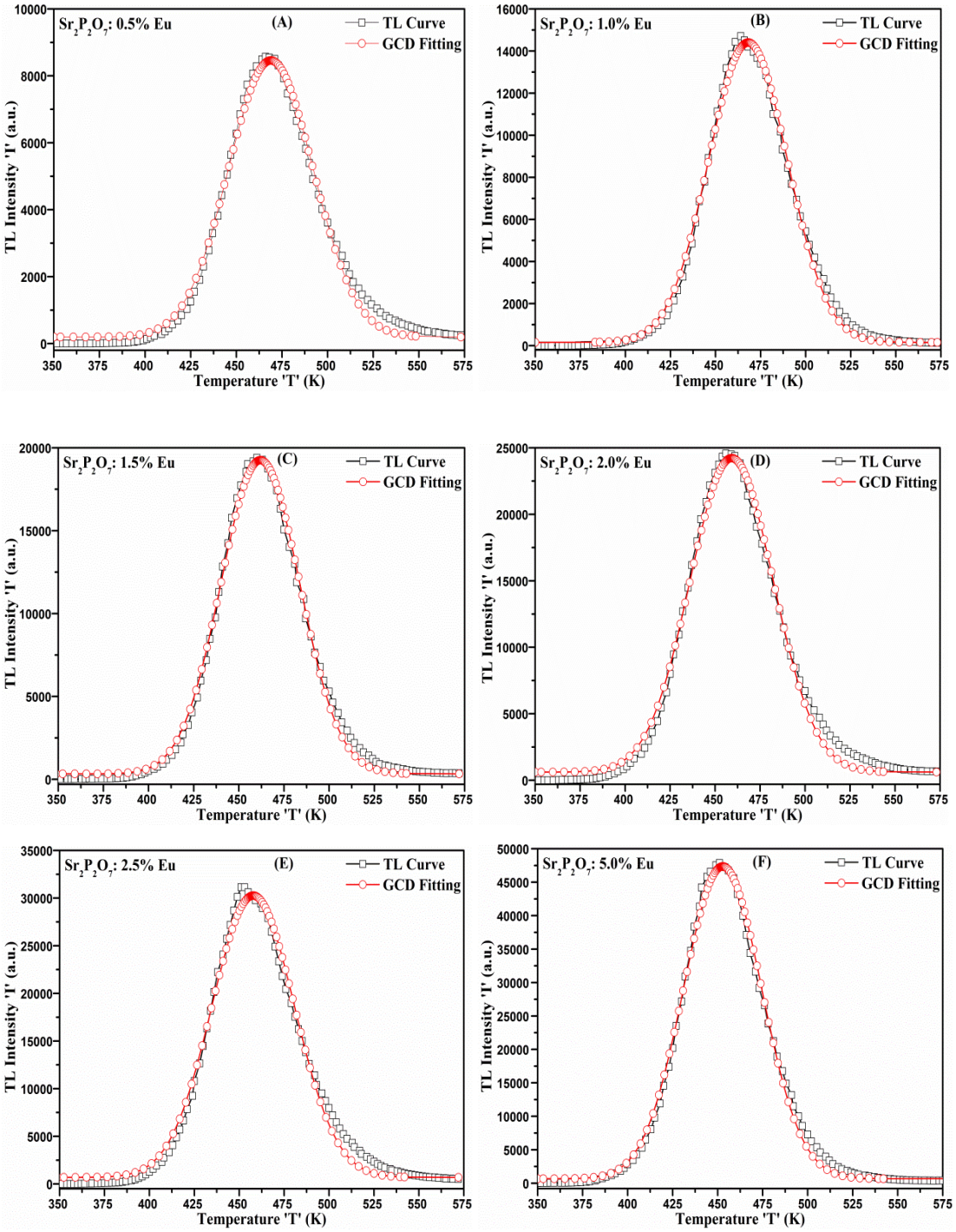

Figure 5.21 GCD fitting of TL glow curves of (A) $Sr_2P_2O_7$: 0.5 mol% Eu^{3+}; (B) $Sr_2P_2O_7$: 1.0 mol% Eu^{3+}; (C) $Sr_2P_2O_7$: 1.5 mol% Eu^{3+}; (D) $Sr_2P_2O_7$: 2.0 mol% Eu^{3+}; (E) $Sr_2P_2O_7$: 2.5 mol% Eu^{3+}; (F) $Sr_2P_2O_7$: 5.0 mol% Eu^{3+}.

Figure 5.20 shows the TL glow curves of Eu^{3+} doped $Sr_2P_2O_7$ carried out after β-irradiation of phosphors by 5 mCi Sr^{90} β-source for different irradiation time, i.e., 0.097 to 0.48 Gy. It shows the TL intensity increases with β-dose that revealed the number electrons trapped at luminescence centers formed in energy gap. TL parameters

of glow of glow such as activation energy, frequency factor, order of kinetics involve in TL mechanism and life time has been calculated by different methods. Figure 5.22 shows the GCD fitting of TL glows of Eu^{3+} doped $Sr_2P_2O_7$ phosphors recorded after 5 minute β- radiation dose. Precise values of figure of merit (FOM) were calculated using equation (16) for experimental and theoretically fitted glow curves. The calculated values of figure of merit (FOM) for different fitted glow curves are mentioned in Table 5.6, which signifies the appropriate fitting of experimental glow curves. GCD fitting of the glow curves have been done through the Kitis et al. equation of second order kinetics given by equation (15). The GCD fitting of the glow curve reveal that the glow curves of 0.5 – 5.0 mol% Eu^{3+} $Sr_2P_2O_7$ follows the second order kinetics, which can identified from the values of order of kinetics 'b' in this method mentioned in Table 5.6. The values of order of kinetics 'b' for each fitted curves are about 1.8 – 2.0, which is the value of second order kinetics. The consistent values of activation energy 'E_a' and frequency factor 's' for electron trap centre in Eu^{3+} doped $Sr_2P_2O_7$ phosphor obtained through GCD method are summarized in Table 5.6. For Eu^{3+} doped $Sr_2P_2O_7$ phosphors the activation energy 'E_a' are ranging from 1.17 – 1.23 eV and frequency factor 's' are of the order of 10^{11} s^{-1}. The TL glow curve parameter also calculated by Chen's peak shape method (PSM) for second order kinetics given by equation (10), (11) and (12). TL parameters calculated by Chen's PSM method for all Eu^{3+} doped $Sr_2P_2O_7$ phosphors are given in Table 5.8. The order of kinetics of TL glow curve is defined from the values of geometric factor 'μ_g'. The values of geometric factor 'μ_g' for Eu^{3+} doped $Sr_2P_2O_7$ phosphors are similar that of the second order kinetics that is nearby 0.52 [102, 104].

The TL glow curve analysis performed by Whole Glow Curve Method and Initial Rise Method. Figure 5.22 (a) shows $\ln[I/(Area)^b]$ vs 1/kT plot of experimental TL outcome of $Sr_2P_2O_7$: 0.5 mol% Eu^{3+} irradiated with dose of β-radiation for 5 minute. The graph has been linearly fitted for different values of order of kinetics '*b*' between 1.8 and 2.1 according to the equation (3) given by whole glow peak method. The linear fitting of experimental TL data of Eu^{3+} doped $Sr_2P_2O_7$ signifies that the glow curve follows the second-order kinetics as studied in GCD analysis. In whole glow peak method, the slope of the graph $\ln[TL/(Area)^b]$ vs 1/kT gives information about the activation energy 'E_a' and intercept gives information of frequency factor 's'. Figure

5.22 (b) shows the graph of residue ln[I/(Area)^b] vs 1/kT to analyse the accurate fitting of experimental values.

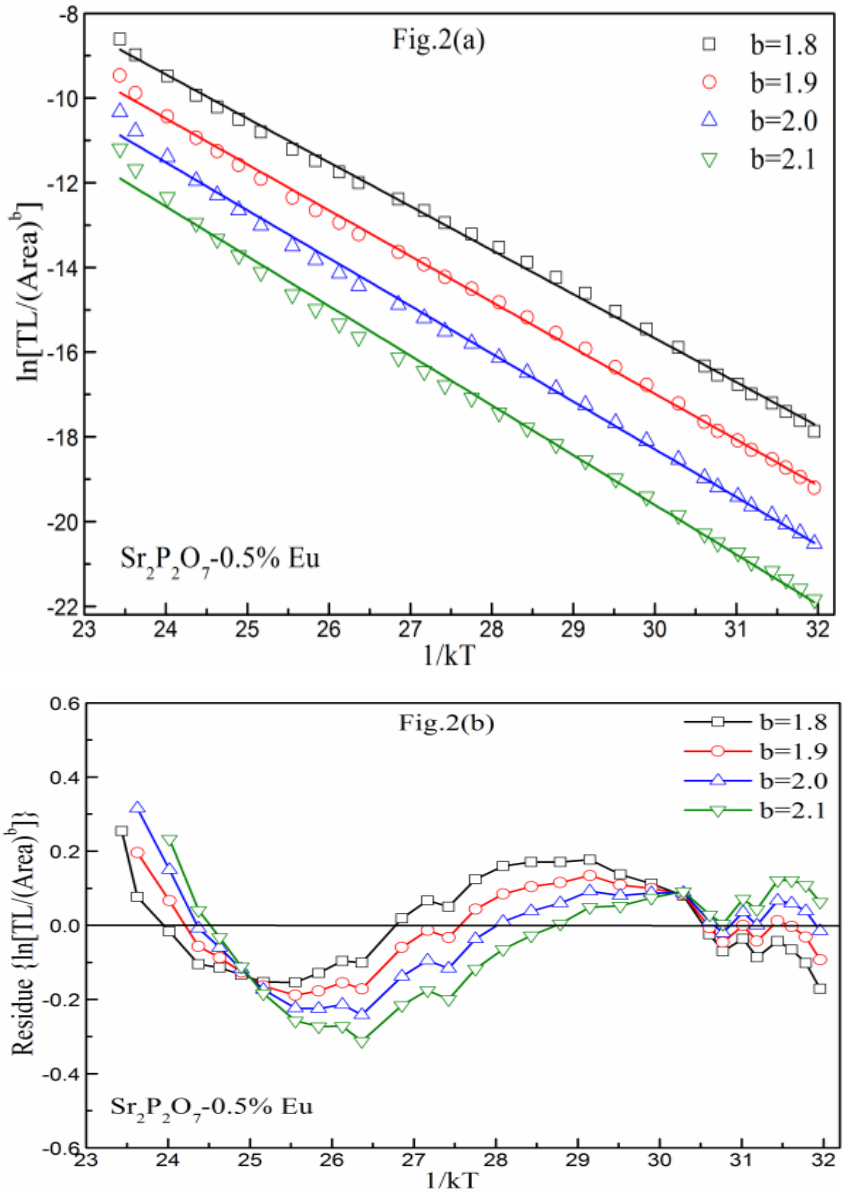

Figure 5.22 (a) ln[TL/(Area)^b] vs 1/kT; (b) Residue ln[TL/(Area)b] vs 1/kT graphs of $Sr_2P_2O_7$:0.5 mol% Eu^{3+} irradiated by β-radiation for 5 minute of 0.48 Gy dose.

As shown in Figure 5.22 (a), the linear fitting for four different values of '*b*' are fairly deviated from straight lines for the low values of 1/kT. The fitted graph for '*b*' value 1.8 displays closely linear relation between theoretical and experimental values which has been analysed by accurate statistical analysis. Whole curve analysis of TL glow curve suggest that the glow curve follows the second order kinetics. Whole glow curve analysis has been performed for all Eu^{3+} doped $Sr_2P_2O_7$ phosphor irradiated with dose of β-radiation for 5 minute. The experimental data of TL glow curve were

consistent within the framework of the whole glow peak method of analysis. It revealed that, the TL glow curves of Eu^{3+} doped $Sr_2P_2O_7$ phosphor follows the second-order kinetics. The values of activation energy 'E_a' and frequency factor 's' for all samples calculated from the graph with best regression fitting line is given in Table 5.7.

Sample	Activation Energy 'E_a' (eV)	Order Of Kinetics 'b'	FOM %	Frequency Factor 's' (s^{-1})
$Sr_2P_2O_7$: 0.5 mol% Eu^{3+}	1.21±0.03	1.8	0.07	3.17×10^{11}
$Sr_2P_2O_7$: 1.0 mol% Eu^{3+}	1.23±0.04	1.9	1.4	1.07×10^{11}
$Sr_2P_2O_7$: 1.5 mol% Eu^{3+}	1.20±0.03	2.0	0.8	2.36×10^{11}
$Sr_2P_2O_7$: 2.0 mol% Eu^{3+}	1.17±0.02	2.0	0.2	1.00×10^{11}
$Sr_2P_2O_7$: 2.5 mol% Eu^{3+}	1.18±0.04	2.0	0.9	3.17×10^{11}
$Sr_2P_2O_7$: 5.0 mol% Eu^{3+}	1.21±0.02	1.9	2.5	2.51×10^{11}

Table 5.6 Summary of TL kinetic parameters of glow curve for sample Eu^{3+} doped $Sr_2P_2O_7$ irradiated by β-radiation for 5 minute of 0.48 Gy dose calculated by GCD method.

Sample	Whole Glow Peak Method			Initial Rise Method	
	Activation Energy (E_a) eV	Order of Kinetics 'b'	Frequency Factor 's' (s^{-1})	Activation Energy (E_a) eV	Frequency Factor 's' (s^{-1})
$Sr_2P_2O_7$: 0.5 mol% Eu^{3+}	1.17±0.02	1.8	3.17×10^{11}	1.16±0.03	5.23×10^{11}
$Sr_2P_2O_7$: 1.0 mol% Eu^{3+}	1.19±0.03	1.9	1.07×10^{11}	1.21±0.04	2.57×10^{11}
$Sr_2P_2O_7$: 1.5 mol% Eu^{3+}	1.15±0.03	2.0	2.36×10^{11}	1.20±0.04	3.54×10^{11}
$Sr_2P_2O_7$: 2.0 mol% Eu^{3+}	1.11±0.03	2.0	1.00×10^{11}	1.14±0.03	2.18×10^{11}
$Sr_2P_2O_7$: 2.5 mol% Eu^{3+}	1.13±0.02	2.0	3.17×10^{11}	1.16±0.03	4.67×10^{11}
$Sr_2P_2O_7$: 5.0 mol% Eu^{3+}	1.15±0.03	1.9	2.51×10^{11}	1.17±0.03	3.78×10^{11}

Table 5.7 Summary of TL glow curves parameters of $Sr_2P_2O_7$: x Eu^{3+} (x = 0.5, 1.0, 1.5, 2.0, 2.5, 5.0 mol%) calculated by Whole Curve Method and Initial Rise Method.

Sample	I_{max}	T_{max} (K)	T_1 (K)	T_2 (K)	τ (K)	δ (K)	ω (K)	μ_g	Activation Energy		
									E_τ (eV)	E_δ (eV)	E_ω (eV)
$Sr_2P_2O_7$: 0.5 mol% Eu^{3+}	8571	467	443.5	493	23.5	26	49.5	0.525	1.28±0.03	1.23±0.04	1.26±0.04
$Sr_2P_2O_7$: 1.0 mol% Eu^{3+}	14706	464	441.5	489	22.5	25	47.5	0.526	1.33±0.04	1.26±0.05	1.30±0.03
$Sr_2P_2O_7$: 1.5 mol% Eu^{3+}	19396	461	438.5	486	22.5	25	47.5	0.525	1.30±0.03	1.25±0.03	1.28±0.03
$Sr_2P_2O_7$: 2.0 mol% Eu^{3+}	24570	456	431	484	25	28	53	0.528	1.14±0.02	1.09±0.02	1.12±0.04
$Sr_2P_2O_7$: 2.5 mol% Eu^{3+}	31132	454	429	482	25	28	53	0.528	1.13±0.05	1.08±0.03	1.18±0.03
$Sr_2P_2O_7$: 5.0 mol% Eu^{3+}	47862	451	427	478	24	27	51	0.529	1.17±0.03	1.11±0.04	1.14±0.02

Table 5.8 Summary of TL kinetic parameters for Eu^{3+} doped $Sr_2P_2O_7$ irradiated by β-radiation for 5 minute of 0.48 Gy dose calculated by PSM.

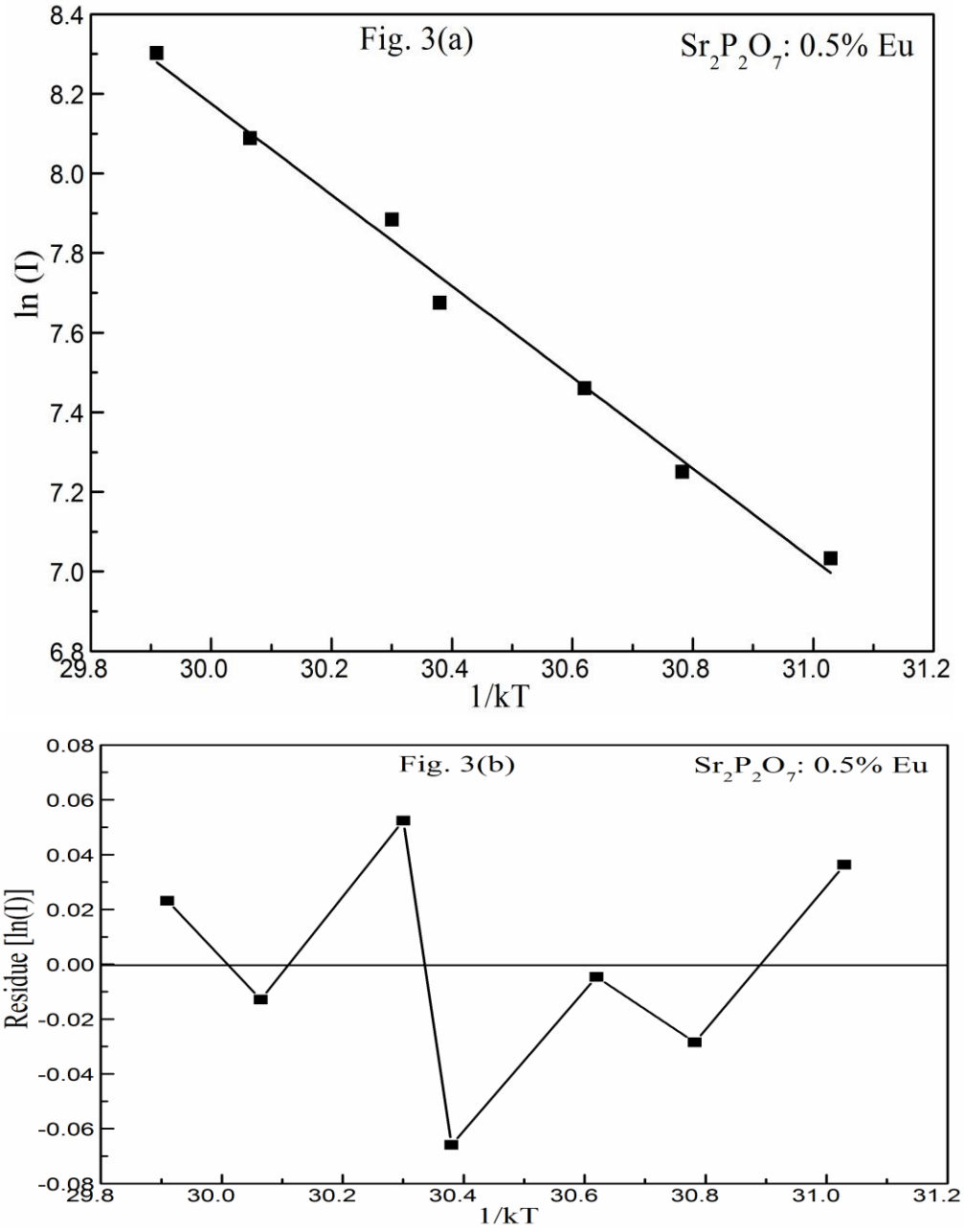

Figure 5.23 (a) ln(I) vs 1/kT; (b) Residue [ln(I)] vs 1/kT graphs of $Sr_2P_2O_7$: 0.5 mol% Eu^{3+} irradiated by β-radiation for 5 minute of 0.48 Gy dose.

Figure 5.23 (a) shows ln(I) vs 1/kT graph for $Sr_2P_2O_7$: 0.5 mol% Eu^{3+} phosphor irradiated by β-radiation for 5 minute, which is straight line for 0.5 mol% Eu^{3+} doping. According to the Initial Rise method the plot of ln(I) vs 1/kT should be straight line as the relation between TL glow curve intensity, temperature and activation energy 'E_a' given by the equation (1). Figure 5.23 (b) shows the graph of residue ln(I) vs 1/kT to examine the precise fitting of experimental values. TL glow curves of all Eu^{3+} doped $Sr_2P_2O_7$ irradiated with dose of β-radiation for 5 minute were analysed by Initial Rise

method. The value of residual factor are very small that signifies the proper fitting of the experimental values. The slope of the straight line gives the value of (E_a/k_B) and the ln(I) - intercept the value of ln(s/β), where β is heating rate for TL glow curve. From the calculation of slope and intercept, activation energy 'E_a' and the frequency factor 's' of TL glow curves were calculated for all Eu^{3+} doped $Sr_2P_2O_7$ phosphors. The calculated values of activation energy and frequency factor through the Initial Rise method were summarized in Table 5.7.

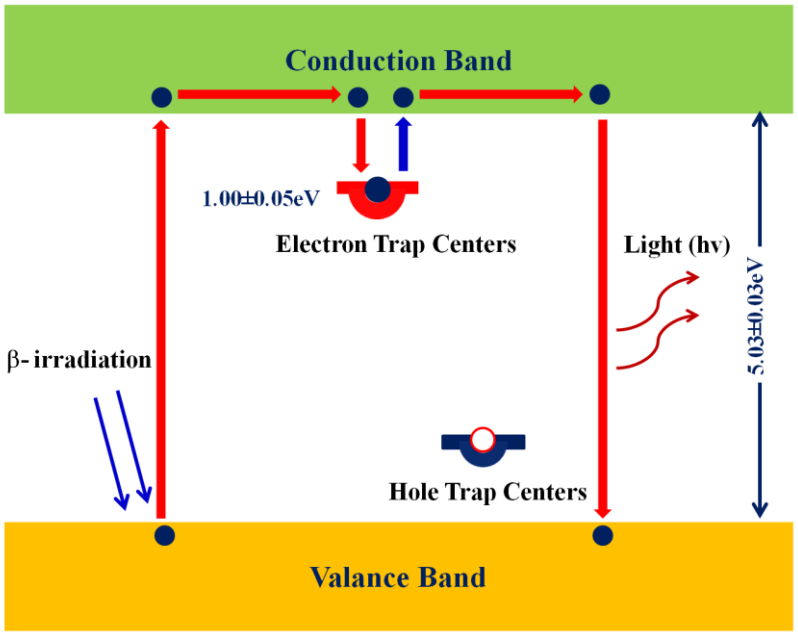

Figure 5.24 Thermoluminescence mechanism involved in Eu^{3+} doped $Sr_2P_2O_7$.

Figure 5.24 shows the band diagram of TL mechanism take place in Eu^{3+} doped $Sr_2P_2O_7$ phosphor β-irradiation. The ionization radiation incident on phosphor can excite the electrons from the valence band of the host which can trapped at metastable energy states or in electron trap centers or localized levels [40, 105]. These trapped electrons does not take part in conduction when the heat energy is supplied to the phosphor this trapped electrons gets free from the trap and recombine with holes in valance band through the conduction band [41, 91, 106]. The energy require to free the electrons from the trap is much lower than that of the energy require to free it from the valence band. The creation of localized energy levels or luminescent centres in energy gap can be induce due to defect or incorporation of intentionally doped impurity within the crystal lattice of host in the form of substitutional or interstitial positions, or cation and anion vacancies.

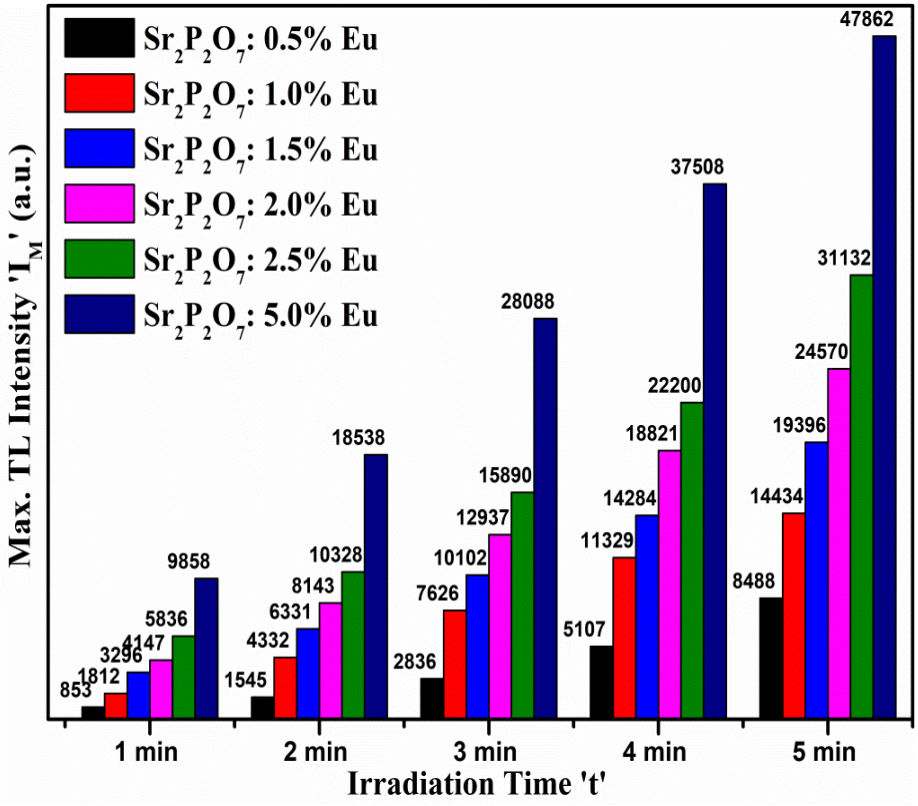

Figure 5.25 Maximum TL intensity 'I_M' vs β-irradiation time 't' graph of Eu^{3+} doped $Sr_2P_2O_7$ irradiated by β-radiation for 5 minute of 0.48 Gy dose.

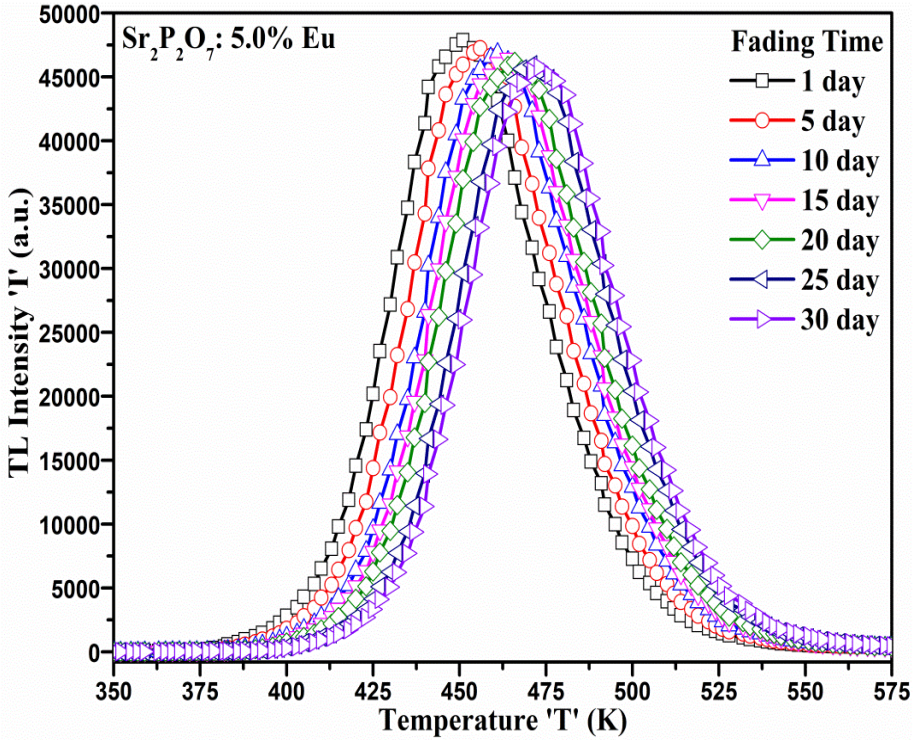

Figure 5.26 TL glow curve of 5.0 mol% Eu^{3+} doped $Sr_2P_2O_7$ for fading time irradiated by β-radiation for 5 minute of 0.48 Gy dose.

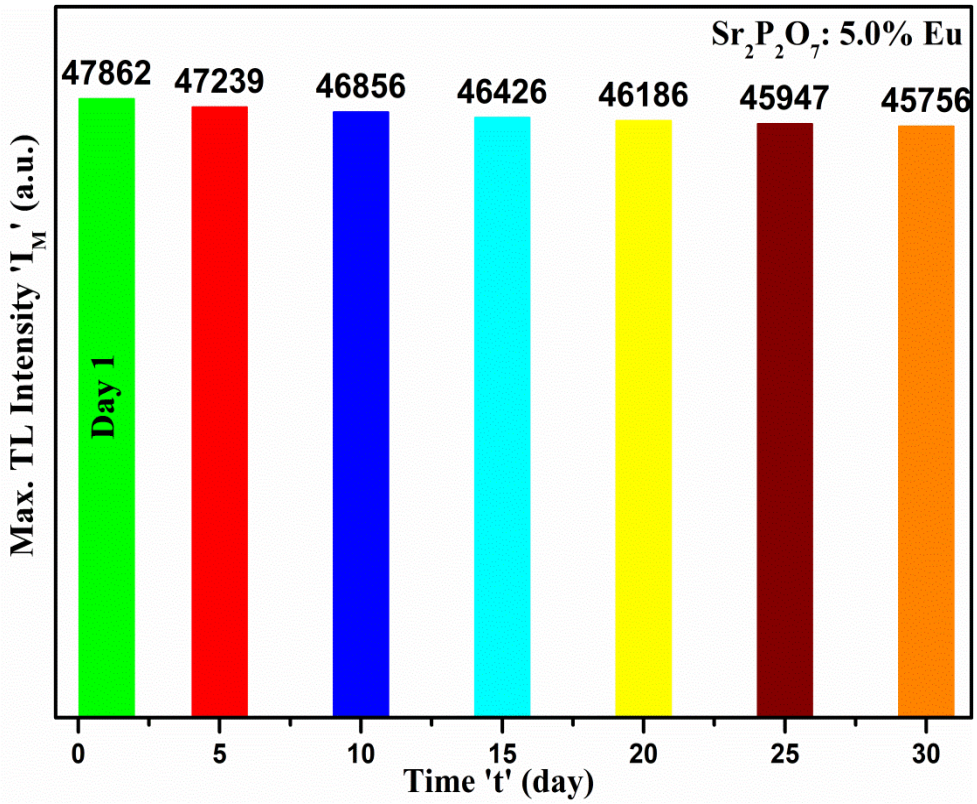

Figure 5.27 Maximum TL intensity 'I_M' vs Fading time 't' graph of 5.0 mol% Eu^{3+} doped $Sr_2P_2O_7$ phosphor irradiated by β-radiation for 5 minute of 0.48 Gy dose.

Figure 5.25 shows Maximum TL intensity vs β-irradiation time graph of Eu^{3+} doped $Sr_2P_2O_7$ for different concentrations of doping ion. The amount of radiation dose and the concentration of dopant prominently affect the TL emission because both the way the trap of electron induced considerably. In Eu^{3+} doped $Sr_2P_2O_7$, it is found that the TL emission intensify as the dose of radiation and doping concentration increase as illustrated in Figure 5.25. TL response after different doses shows linear with β-dose and doping concentration. Figure 5.26 shows the TL glow curve of $Sr_2P_2O_7$: 5.0 mol% Eu^{3+} phosphor recorded at different time after β- irradiation of phosphor for 5 minute to examine the fading effect after exposure, which gives the information about how long the phosphor can store the exposure energy. The fading effect is the one of the most useful characteristic of good TL dosimeter. The TL glow curves were acquired to analyze the fading effect of TL glow curve for one month at interval of five days for one month for all samples. The phosphors were stored in dark condition at room temperature after exposure of β-radiation. This fading study showed that the TL glow curve peak temperature 450 K is shifted towards higher temperature up to 465 K in the time period of one month, but the fading of Peak maximum is much low. Similar kind

of fading effect were observed in all samples with different concentration and doses. Figure 5.27 shows Maximum TL intensity vs Fading time graph of $Sr_2P_2O_7$: 5.0% Eu^{3+} phosphor irradiated by β- radiation for 5 minute.

5.3.4. $Sr_2P_2O_7$: Dy^{3+}

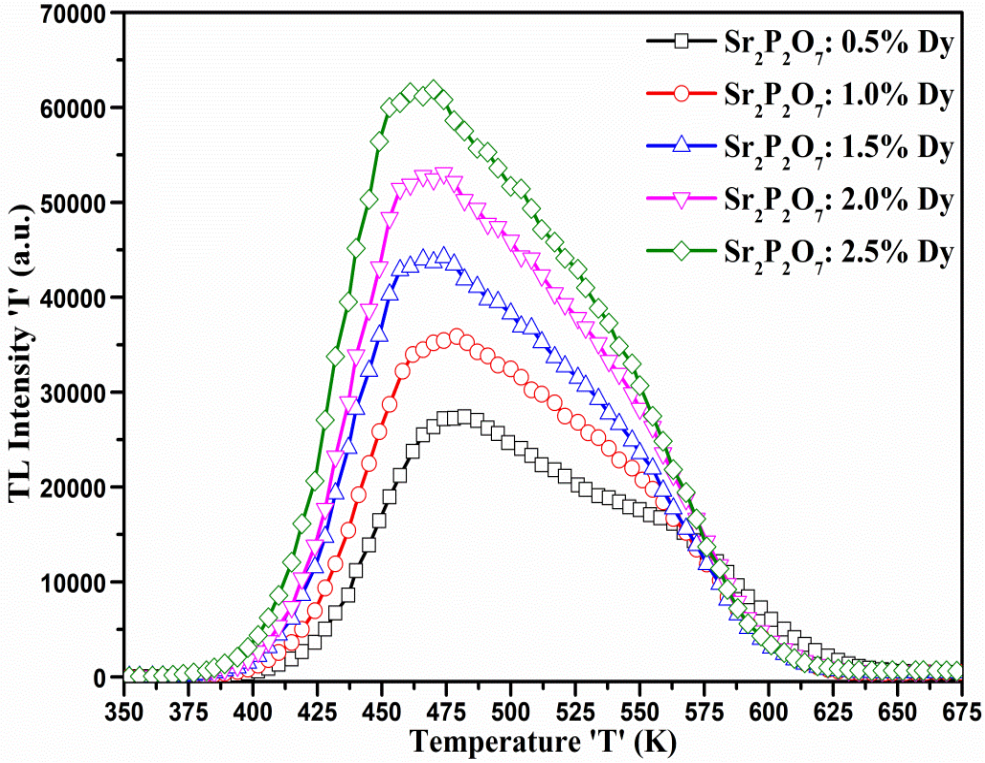

Figure 5.28 TL glow curve of $Sr_2P_2O_7$: x Dy^{3+} (x = 0.5, 1.0, 1.5, 2.0, 2.5 mol%) phosphors irradiated by β-radiation for 5 minute of 0.48 Gy dose.

Figure 5.28 shows the glow curves of Dy^{3+} doped $Sr_2P_2O_7$ exposed to β-radiation for 5 minute and dose of 0.48 Gy for various concentrations of doping. From the TL curve it can be perceived that a single broad TL peak is experiential for all doped $Sr_2P_2O_7$ phosphors. TL intensity of glow curve increases with doping concentration however there is a shift of glow curve occur towards the lower temperature with the increasing doping concentration of Dy^{3+} ions. This could be resulting due to the change in doping concentration affecting the trap levels of the phosphor. The increase in the activator concentration increases the energy stored by the ions, consequently the TL intensity also increases. The maximum TL intensity is obtained at 2.5 mol% Dy^{3+} concentration. The concentration quenching effect cannot observed for the value of highest concentration of 2.5 mol% of Dy^{3+}. Figure 5.29 shows the TL glow curves of Dy^{3+} ion doped $Sr_2P_2O_7$ phosphor exposed to β-radiation for 5

minute. The graph of TL glow curves illustrates that as the concentration of activator ion and dose amount are progressively increase the electron traps, thus the TL intensity also increases accordingly [101, 107].

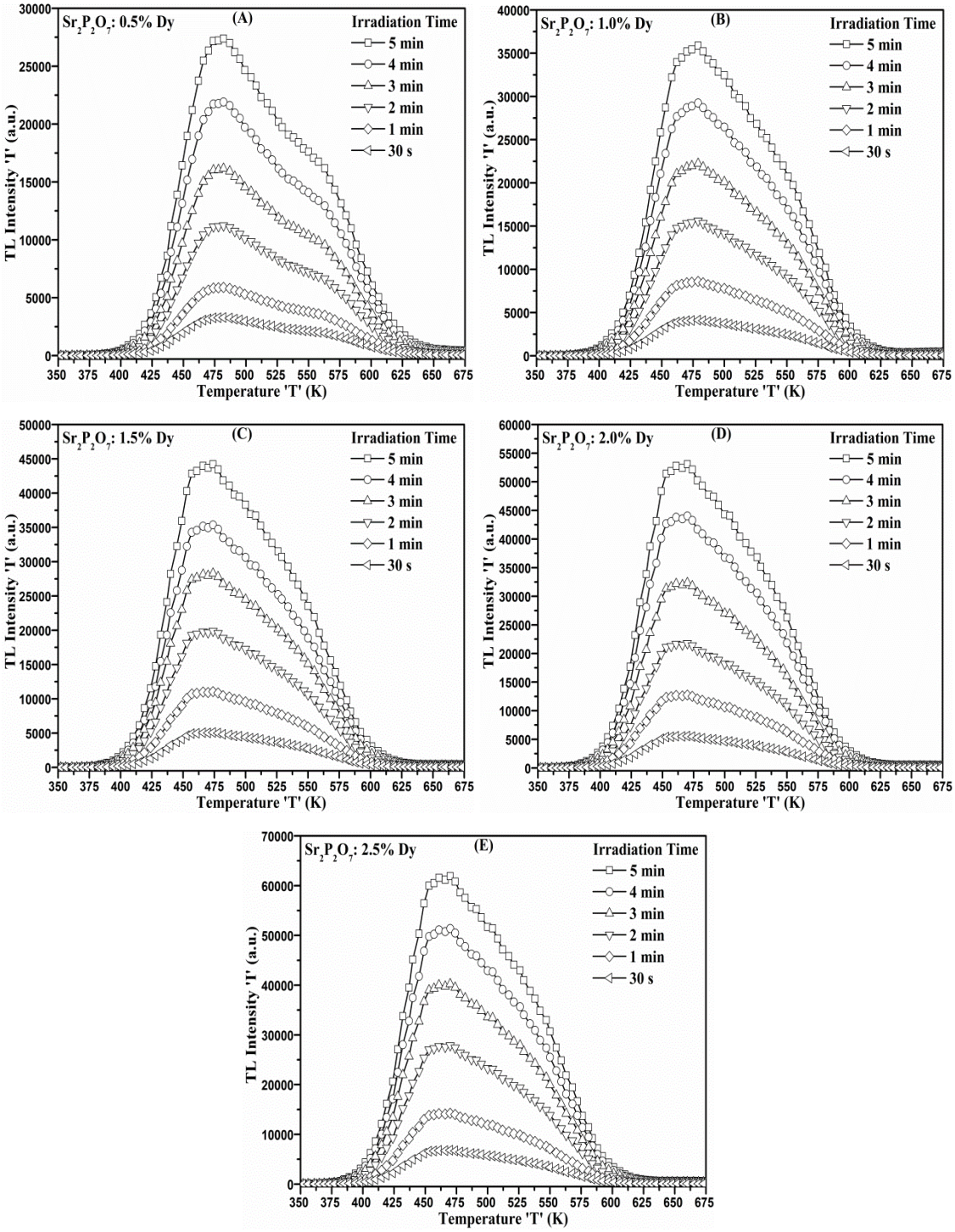

Figure 5.29 TL glow curve for various time of β-irradiation: (A) $Sr_2P_2O_7$: 0.5 mol% Dy^{3+}; (B) $Sr_2P_2O_7$: 1.0 mol% Dy^{3+}; (C) $Sr_2P_2O_7$: 1.5 mol% Dy^{3+}; (D) $Sr_2P_2O_7$: 2.0 mol% Dy^{3+}; (E) $Sr_2P_2O_7$: 2.5 mol% Dy^{3+}.

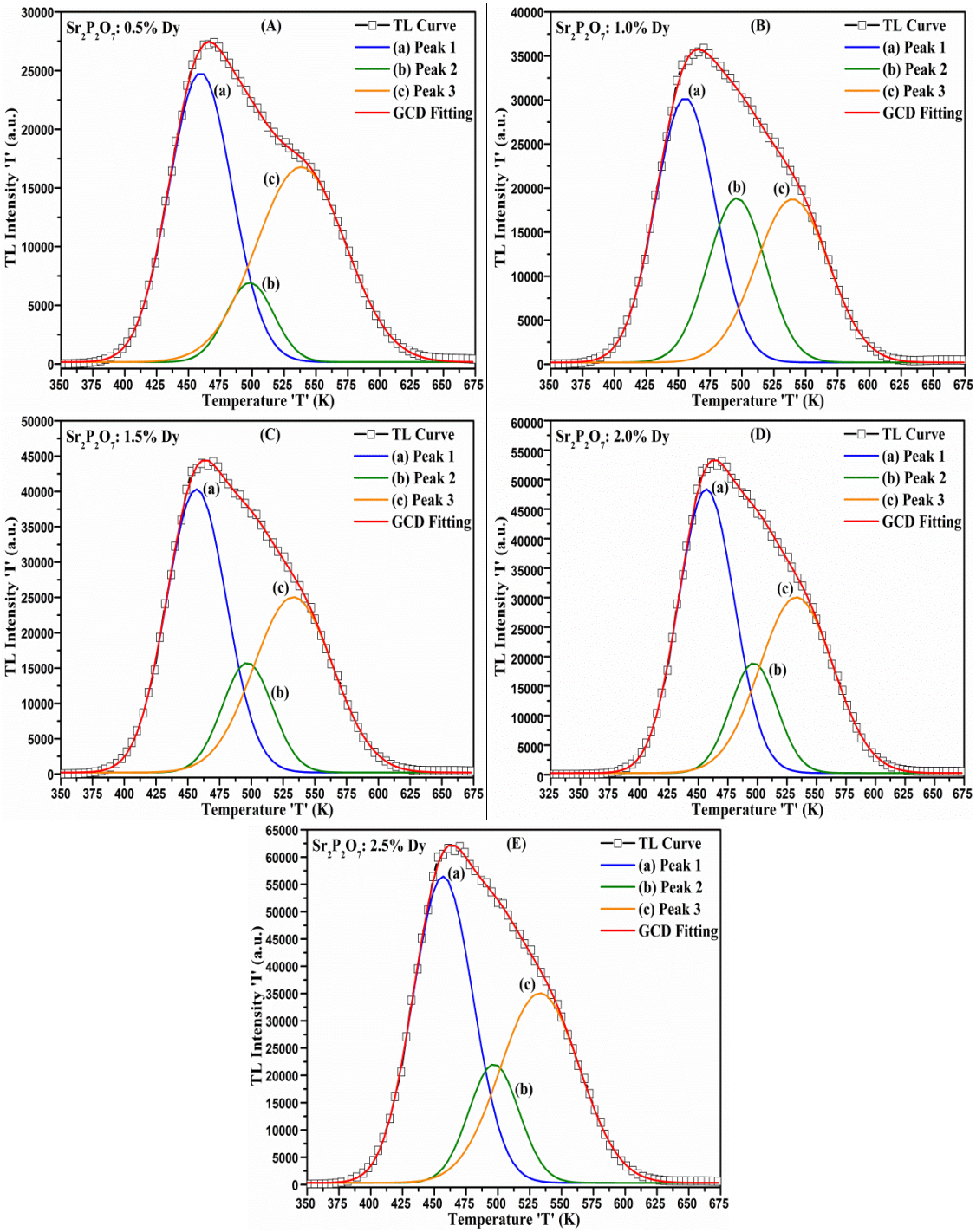

Figure 5.30 GCD fitting of TL glow curves of (A) $Sr_2P_2O_7$: 0.5 mol% Dy^{3+}; (B) $Sr_2P_2O_7$: 1.0 mol% Dy^{3+}; (C) $Sr_2P_2O_7$: 1.5 mol% Dy^{3+}; (D) $Sr_2P_2O_7$: 2.0 mol% Dy^{3+}; (E) $Sr_2P_2O_7$: 2.5 mol% Dy^{3+}.

TL parameters of glow curves such as activation energy, frequency factor, order of kinetics involve in TL mechanism have been calculated by GCD method and PSM method. Figure 5.30 shows the GCD fitting of TL glows of Dy^{3+} doped $Sr_2P_2O_7$ phosphor recorded after 5 minute for the 0.48 Gy dose of β-radiation. GCD fitting of

the glow curves have been done through the Kitis et al. equation of second order kinetics given by equation (15). The experimental TL glove curve fitting was achieved by minimizing the value of figure of merit. Fine value of figure of merit (FOM) were calculated using equation (16) for experimental and theoretically fitted glow corves. Figure of merit (FOM) for fitted glow curve of 2.5 mol% Dy^{3+} doped $Sr_2P_2O_7$ is mentioned in Table 5.9, which is small for fine fitting curves, which be a sign of the appropriate fitting of experimental glow curves. From the GCD analysis, it is perceived that the TL glove curve of 2.5 mol% Dy^{3+} doped $Sr_2P_2O_7$ phosphors comprises of three peak with peak temperature around 457, 496 and 536 K. The GCD fitting of the glow curve reveal that the glow curves of 0.5 – 2.5 mol % Dy^{3+} doped $Sr_2P_2O_7$ phosphors follow the second order kinetics, which can identified from the values of order of kinetics 'b' in this method mentioned in Table 5.9. The values of order of kinetics 'b' for peak I, II, III are about 1.8, 2.0 and 2.1, which is the value of second order kinetics. The activation energy 'E_a' found for the peaks are of the range from 0.9 – 1.6 eV and the frequency factor 's' is of the order of 10^{10} – 10^{12} s^{-1}. The consistent values of activation energy 'E_a' and frequency factor 's' for electron trap centre in Dy^{3+} doped $Sr_2P_2O_7$ phosphor obtained through GCD method are summarized in Table 5.9. The TL glow curve parameter also calculated by Chen's peak shape method (PSM) for second order kinetics given by equation (10), (11) and (12). TL parameters calculated by Chen's PSM method for all 2.5 mol% Dy^{3+} doped $Sr_2P_2O_7$ phosphors are given in Table 5.10. The calculated values of activation energy for all Dy^{3+} through PSM are very significant that of the values of GCD method. The order of kinetics of TL glow curve is defined from the values of geometric factor 'μ_g'. The values of geometric factor 'μ_g' for Dy^{3+} doped $Sr_2P_2O_7$ phosphors are similar that of the second order kinetics that is nearby 0.52 [107].

Figure 5.31 shows Maximum TL intensity vs β-irradiation time graph of Dy^{3+} doped $Sr_2P_2O_7$ for different concentrations of doping ion. As mentioned in above RE^{3+} doped $Sr_2P_2O_7$, TL intensity depends on the amount of dose absorbed by the phosphor and doping concentration. Dy^{3+} doped $Sr_2P_2O_7$ also show similar nature as mentioned above and TL emission increases with the dose of radiation and doping concentration increase as illustrated in Figure 5.31. Figure 5.32 shows the TL glow curves of $Sr_2P_2O_7$: 2.5 mol% Dy^{3+} phosphor recorded at different time after β- irradiation to examine the fading effect after exposure. It shows only 1-2% of fading in maximum TL intensity per

five day observation as well as the peak shifting toward higher temperature. The fading effect is the one of the most useful characteristic of good TL dosimeter. The TL glow curves were acquired for one month at interval of five days for one month for all samples. The phosphors were stored in dark condition at room temperature after exposure of β-radiation.

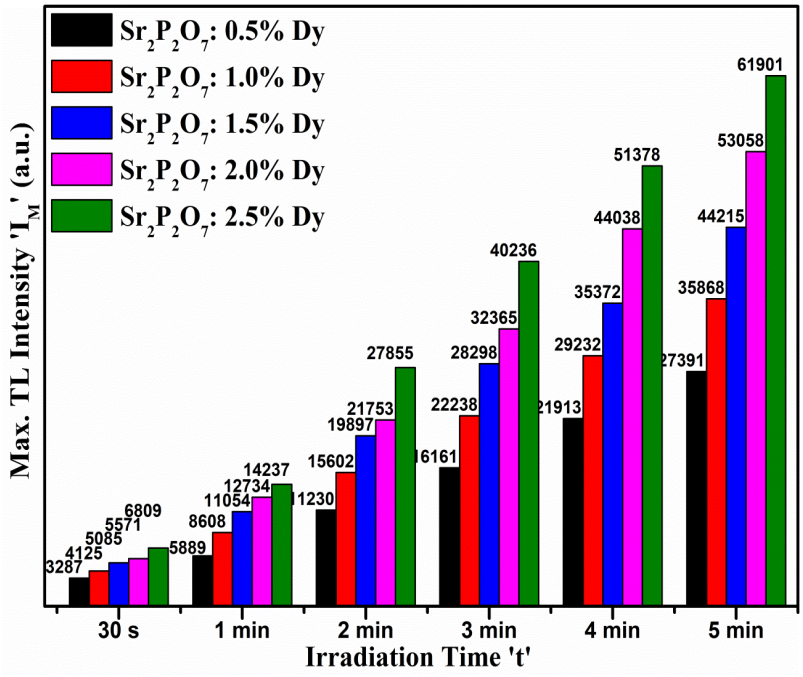

Figure 5.31 Maximum TL intensity 'I_M' vs β-irradiation time 't' graph of Dy^{3+} doped $Sr_2P_2O_7$ irradiated by β-radiation for 5 minute of 0.48 Gy dose..

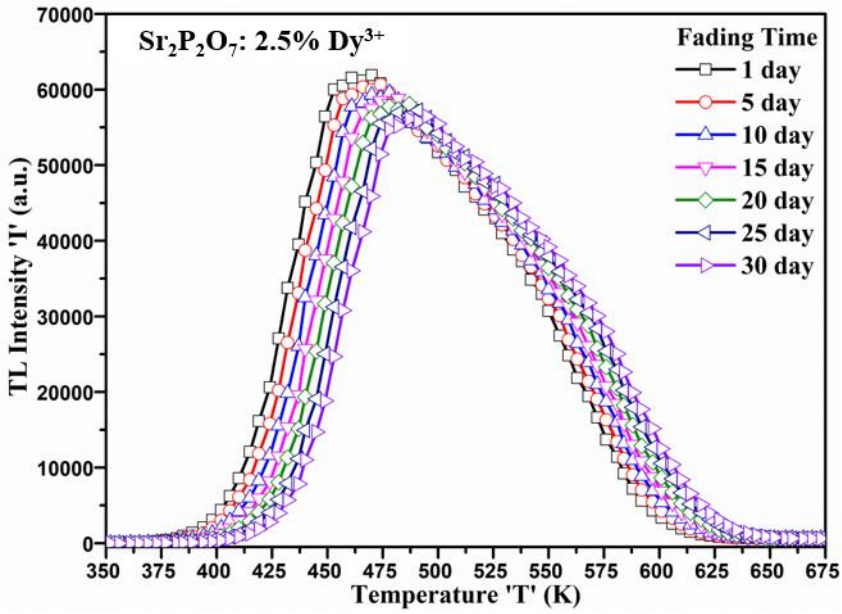

Figure 5.32 TL glow curve of 2.5 mol% Dy^{3+} doped $Sr_2P_2O_7$ for fading time irradiated by β-radiation for 5 minute of 0.48 Gy dose.

This fading study showed that the TL glow curve peak temperature 450 K is shifted towards higher temperature up to 465 K in the time period of one month, but the fading of Peak maximum is much low. Similar kind of fading effect were observed in all samples with different concentration and doses. Figure 5.33 shows Maximum TL intensity vs Fading time graph of $Sr_2P_2O_7$: 2.5 mol% Dy^{3+} phosphor irradiated by β-particle for 5 minute.

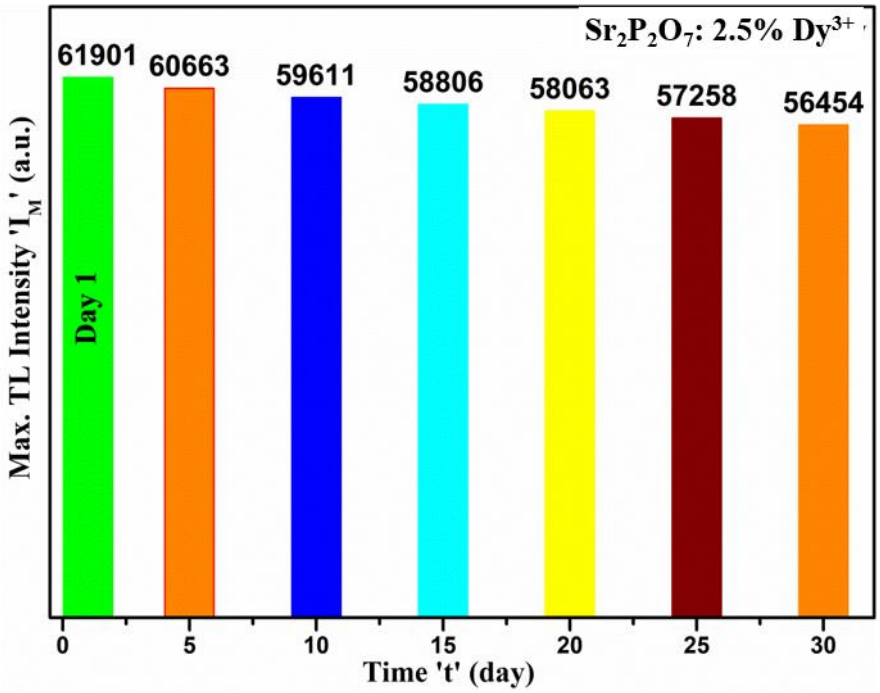

Figure 5.33 Maximum TL intensity 'I_M' vs Fading time 't' graph of 2.5 mol% Dy^{3+} doped $Sr_2P_2O_7$ phosphor irradiated by β-radiation for 5 minute of 0.48 Gy dose.

Sample	Activation Energy 'E_a' (eV)	Order Of Kinetics 'b'	FOM %	Frequency Factor 's' (s^{-1})
$Sr_2P_2O_7$: 2.5 mol% Dy^{3+}	1.12±0.02	1.8	0.17	3.11×10^{10}
	1.49±0.04	2.0		1.23×10^{12}
	1.07±0.03	2.1		2.89×10^{11}

Table 5.9 Summary of TL kinetic parameters of glow curve for sample 2.5 mol% Dy^{3+} doped $Sr_2P_2O_7$ irradiated by β-radiation for 5 minute of 0.48 Gy dose calculated by GCD method.

Sample	T_{max} (K)	T_1 (K)	T_2 (K)	τ (K)	δ (K)	ω (K)	μ_g	Activation Energy		
								E_τ (eV)	E_δ (eV)	E_ω (eV)
$Sr_2P_2O_7$: 0.5 mol% Dy^{3+}	457	428.5	489	28.5	32	60.5	0.528	0.98±0.03	0.96±0.04	0.97±0.04
	499	477	522	22	23	45	0.511	1.59±0.04	1.59±0.05	1.60±0.03
	538	498	580	40	42	82	0.512	0.94±0.03	1.01±0.03	0.98±0.03
$Sr_2P_2O_7$: 1.0 mol% Dy^{3+}	454	428	483	26	29	55	0.527	1.07±0.02	1.04±0.02	1.06±0.04
	495	468	524	27	29	56	0.517	1.24±0.05	1.24±0.03	1.24±0.03
	538	505	574	33	36	69	0.521	1.18±0.03	1.18±0.04	1.18±0.02
$Sr_2P_2O_7$: 1.5 mol% Dy^{3+}	457	429	487	28	30	58	0.517	1.00±0.03	1.02±0.04	1.01±0.04
	496	473	521	23	25	48	0.520	1.49±0.04	1.45±0.05	1.47±0.03
	534	497	573	37	39	76	0.513	1.01±0.03	1.07±0.03	1.05±0.03
$Sr_2P_2O_7$: 2.0 mol% Dy^{3+}	457	428	489	29	32	61	0.524	0.96±0.03	0.96±0.04	0.96±0.04
	497	474	522	23	25	48	0.521	1.37±0.04	1.32±0.05	1.33±0.03
	534	496	575	38	41	79	0.518	0.98±0.03	1.02±0.03	1.00±0.03
$Sr_2P_2O_7$: 2.5 mol% Dy^{3+}	457	431	485	26	28	54	0.518	1.09±0.02	1.09±0.02	1.10±0.04
	496	471	523	25	27	52	0.519	1.36±0.05	1.34±0.03	1.35±0.03
	534	497	573	37	39	76	0.513	1.01±0.03	1.07±0.04	1.05±0.02

Table 5.10 Summary of TL kinetic parameters for Dy^{3+} doped $Sr_2P_2O_7$ irradiated by β-radiation for 5 minute of 0.48 Gy dose calculated by PSM.

As the incorporation of RE^{3+} ions takes place at Sr^{2+} ions sites in host, i.e., divalent host ion substituted by trivalent impurity ion, necessitates the charge compensatory vacancy because of charge imbalance occur in host. In charge compensation procedure two RE^{3+} ions can be substitute three Sr^{2+} ions, where two RE^{3+} ions occupy at two strontium sites and leaving a one-site empty, **[108]**. These could be results into the formation of one vacancy in the lattices and incorporation of RE^{3+} ions results in two types of sites for RE^{3+} ions in host $Sr_2P_2O_7$ **[108]**. When two RE^{3+} ion substitutes three Sr^{2+} ion in the two different lattice site of $Sr_2P_2O_7$ host, two substitutional defect produce due to the RE^{3+} ion which is positive and acts as electron trap. As the concentration of doping ions increases the incorporation of RE^{3+} on a Sr^{2+} site increases prominently and the density of electron trap increases considerably, which can enhance the TL properties of the phosphor.

Thermoluminescence Output of RE^{3+} doped $Sr_2P_2O_7$

Thermoluminescence (TL) studies of RE^{3+} doped $Sr_2P_2O_7$ phosphor were cried out after β-irradiation by Sr^{90} source. Ce^{3+} doped $Sr_2P_2O_7$ phosphor showed the maximum TL emission at around 383 K temperature. Eu^{3+} doped $Sr_2P_2O_7$ phosphor showed the maximum TL emission at around 460 K temperature. Tb^{3+} doped $Sr_2P_2O_7$ phosphor showed the maximum TL emission at around 425 K and other peak intensity at around 560 K temperature. Dy^{3+} doped $Sr_2P_2O_7$ phosphor showed the maximum TL emission at around 465 K temperature. Out of all four RE^{3+} doped $Sr_2P_2O_7$ phosphors, Eu^{3+} and Dy^{3+} doped phosphor showed maximum TL intensity of about 50000 units, which is a good TL outcome. TL glow curve intensity of RE^{3+} doped $Sr_2P_2O_7$ phosphors increases linearly with doping concentration and exposure dose. The fading of the TL intensity is very low for the storage of 30 day, which is less than 7%. The reusability of the phosphor were studied for ten cycles, which is consistent for each use for exposure. All the phosphors are very sensitive to the lower doses. The TL parameters obtained for different RE^{3+} doped $Sr_2P_2O_7$ phosphors are very consistent and nearby the traditional TLDs. The results suggests that the RE^{3+} doped phosphors be the potential for environmental dosimetry and accidental dosimetry applications.

References

1. Mckeever, S., *Thermoluminescence of Solids. Department of Physics, Oklahoma state university*, 1985, Cambridge University press.
2. Bhatt, B. and M. Kulkarni. *Thermoluminescent phosphors for radiation dosimetry*. in *Defect and Diffusion Forum*. 2014. Trans Tech Publ.
3. Harvey, E.N., *A history of luminescence from the earliest times until 1900*. Vol. 44. 1957: American Philosophical Society.
4. Sunta, C., *Unraveling Thermoluminescence*. Vol. 202. 2014: Springer.
5. Cairns, T., *Archaeological dating by thermoluminescence.* Analytical Chemistry, 1976. **48**(3): p. 266A-280a.
6. McKeever, S. and R. Chen, *Luminescence models.* Radiation Measurements, 1997. **27**(5-6): p. 625-661.
7. Kragh, H., *Phosphors and Phosphorous in Early Danish Natural Philosophy.* 2003.
8. Walsh, P. and E. Lightowlers, *The application of thermoluminescence theory to natural semiconducting diamond.* Journal of Luminescence, 1971. **4**(4): p. 393-403.
9. Hornyak, W., R. Chen, and A. Franklin, *Thermoluminescence characteristics of the 375 C electron trap in quartz.* Physical Review B, 1992. **46**(13): p. 8036.
10. Horowitz, Y., et al., *Thermoluminescence Theory and Analysis: Advances and Impact on Applications.* 2017.
11. Garlick, G. and A. Gibson, *The electron trap mechanism of luminescence in sulphide and silicate phosphors.* Proceedings of the physical society, 1948. **60**(6): p. 574.
12. Vass, I., *The history of photosynthetic thermoluminescence.* Photosynthesis research, 2003. **76**(1-3): p. 303-318.
13. Chen, R. and S.W. McKeever, *Theory of thermoluminescence and related phenomena*, 1997: World Scientific.
14. Bos, A., *Theory of thermoluminescence.* Radiation measurements, 2006. **41**: p. S45-S56.
15. Alexander, C. and S. McKeever, *Phototransferred thermoluminescence.* Journal of Physics D: Applied Physics, 1998. **31**(20): p. 2908.

16. Wiedemann, E. and G.K. Schmidt, *Ueber luminescenz*, 1895: Johann Ambrosius Barth (Arthur Meiner).
17. Kron, T., *Thermoluminescence dosimetry and its applications in medicine--Part 2: History and applications.* Australasian physical & engineering sciences in medicine, 1995. **18**(1): p. 1-25.
18. Kron, T., *Applications of thermoluminescence dosimetry in medicine.* Radiation protection dosimetry, 1999. **85**(1-4): p. 333-340.
19. Blanchard, F., *Thermoluminescence of fluorite and age of deposition.* American Mineralogist, 1966. **51**(3-4): p. 474-+.
20. Curie, M., *Radio-active substances*. Vol. 2. 1904: Chemical News Office.
21. Bradley, D., et al., *Review of doped silica glass optical fibre: their TL properties and potential applications in radiation therapy dosimetry.* Applied Radiation and Isotopes, 2012. **71**: p. 2-11.
22. Ghormley, J. and H. Levy, *Some Observations of Luminescence of Alkali Halide Crystals Subjected to Ionizing Radiation.* The Journal of Physical Chemistry, 1952. **56**(5): p. 548-554.
23. Rappaport, F. and J. Lavergne, *Thermoluminescence: theory.* Photosynthesis research, 2009. **101**(2-3): p. 205-216.
24. Haake, C., *Critical comment on a method for determining electron trap depths.* JOSA, 1957. **47**(7): p. 649-652.
25. Claudio, F., *Handbook of Thermoluminescence*, 2009: World Scientific.
26. Medlin, W., *Trapping centers in thermoluminescent calcite.* Physical Review, 1964. **135**(6A): p. A1770.
27. Roth, E. and B. Poty, *Nuclear methods of dating*, 1989.
28. Bhatt, B.C., *Thermoluminescence, optically stimulated luminescence and radiophotoluminescence dosimetry: An overall perspective.* Radiation Protection and Environment, 2011. **34**(1): p. 6.
29. Bøtter-Jensen, L., S.W. McKeever, and A.G. Wintle, *Optically stimulated luminescence dosimetry*, 2003: Elsevier.
30. Pradhan, A., J. Lee, and J. Kim, *Recent developments of optically stimulated luminescence materials and techniques for radiation dosimetry and clinical applications.* Journal of Medical Physics/Association of Medical Physicists of India, 2008. **33**(3): p. 85.

31. Andreo, P., et al., *Absorbed dose determination in photon and electron beams. An international Code of Practice.* 1987.
32. Piters, T.M., *A study into the mechanism of thermoluminescence in a LiF: Mg, Ti dosimetry material*, 1993: Delft University of Technology.
33. Sekkina, M., et al., *Thermoluminescence archaeological dating of pottery in the Egyptian pyramids zone.* Ceramics-Silikaty, 2003. **47**(3): p. 94-99.
34. Blasse, G. and B. Grabmaier, *Luminescent materials*, 2012: Springer Science & Business Media.
35. Prasad, A.K., et al., *Optical dating in a new light: A direct, non-destructive probe of trapped electrons.* Scientific reports, 2017. **7**(1): p. 12097.
36. Aboud, H., H. Wagirana, and R. Hussina, *Mechanism of Thermoluminescence.* Int. J. Scie. Engi Res, 2012. **3**: p. 650-65.
37. Betts, D. and P. Townsend, *Temperature distribution in thermoluminescence experiments. II. Some calculational models.* Journal of Physics D: Applied Physics, 1993. **26**(5): p. 849.
38. McKeever, S., *Luminescence dosimetry: recent developments in theory and applications.* 2000.
39. Pranaitis, M., et al., *Gaussian Distribution of the Charge Traps in the Energy Gap of MDMO-PPV and Its Dependence on Synthesis Route Revealed by the Thermally Stimulated Current Spectroscopy.* Molecular Crystals and Liquid Crystals, 2014. **604**(1): p. 96-106.
40. Murthy, K. and H.S. Virk. *Luminescence phenomena: an introduction*. in *Defect and Diffusion Forum*. 2014. Trans Tech Publ.
41. Bos, A.J., *Thermoluminescence as a Research Tool to Investigate Luminescence Mechanisms.* Materials, 2017. **10**(12): p. 1357.
42. Zhang, Y., *Electronic structures of impurities and point defects in semiconductors.* arXiv preprint arXiv:1709.04058, 2017.
43. Nambi, K., *Thermoluminescence: Its understanding and applications*, 1977, Instituto de Energia Atomica.
44. Aitken, M.J., *Introduction to optical dating: the dating of Quaternary sediments by the use of photon-stimulated luminescence*, 1998: Clarendon Press.
45. Gupta, K. and N. Gupta, *Advanced semiconducting materials and devices*, 2016: Springer.

46. Wintle, A. and D. Huntley, *Thermoluminescence dating of a deep-sea sediment core.* Nature, 1979. **279**(5715): p. 710.
47. Lany, S. and A. Zunger, *Anion vacancies as a source of persistent photoconductivity in II-VI and chalcopyrite semiconductors.* Physical Review B, 2005. **72**(3): p. 035215.
48. Lischka, K., *Deep level defects in narrow gap semiconductors.* physica status solidi (b), 1986. **133**(1): p. 17-46.
49. Fox, M., *Optical properties of solids*, 2002, AAPT.
50. Hummel, R.E., *Introduction*, in *Electronic Properties of Materials*, 2011, Springer. p. 405-407.
51. Zhang, Z. and J.T. Yates Jr, *Band bending in semiconductors: chemical and physical consequences at surfaces and interfaces.* Chemical reviews, 2012. **112**(10): p. 5520-5551.
52. Horowitz, Y.S., *Thermoluminescence and Thermoluminescent Dosimetry, v. 2.* 1984.
53. Townsend, P. and A. Rowlands, *Extended defect models for thermoluminescence.* Radiation Protection Dosimetry, 1999. **84**(1-4): p. 7-12.
54. Turkin, A., et al., *Thermoluminescence of zircon: a kinetic model.* Journal of Physics: Condensed Matter, 2003. **15**(17): p. 2875.
55. Rodnyi, P., P. Dorenbos, and C. Van Eijk, *Energy loss in inorganic scintillators.* physica status solidi (b), 1995. **187**(1): p. 15-29.
56. Izewska, J. and G. Rajan, *Radiation dosimeters.* Radiation Oncology Physics: A Handbook for Teachers and Students, 2005: p. 71-99.
57. McKeever, S.W., M. Moscovitch, and P.D. Townsend, *Thermoluminescence dosimetry materials: properties and uses.* 1995.
58. Furetta, C., *Handbook of thermoluminescence*, 2010: World Scientific.
59. Kirsh, Y., *Kinetic analysis of thermoluminescence.* physica status solidi (a), 1992. **129**(1): p. 15-48.
60. Chen, R., D. Huntley, and G. Berger, *Analysis of Thermoluminescence Data Dominated by Second-Order Kinetics.* physica status solidi (a), 1983. **79**(1): p. 251-261.

61. Chen, R., V. Pagonis, and J. Lawless, *Evaluated thermoluminescence trapping parameters–What do they really mean?* Radiation Measurements, 2016. **91**: p. 21-27.
62. Pagonis, V. and G. Kitis, *Prevalence of first-order kinetics in thermoluminescence materials: An explanation based on multiple competition processes.* physica status solidi (b), 2012. **249**(8): p. 1590-1601.
63. Pagonis, V., G. Kitis, and C. Furetta, *Analysis of Thermoluminescence Data.* Numerical and Practical Exercises in Thermoluminescence, 2006: p. 23-78.
64. Chen, R., *Methods for kinetic analysis of thermally stimulated processes.* Journal of Materials Science, 1976. **11**(8): p. 1521-1541.
65. Kitis, G. and V. Pagonis, *Peak shape methods for general order thermoluminescence glow-peaks: a reappraisal.* Nuclear Instruments and Methods in Physics Research Section B: Beam Interactions with Materials and Atoms, 2007. **262**(2): p. 313-322.
66. Patel, N.P., et al., *Investigation of dosimetric features of beta–irradiated* Er^{3+} *doped strontium pyrophosphate, 2015.*
67. Rao, M.R., et al., *Thermoluminescence characteristics of* MgB_4O_7, MgB_4O_7*: Mn and* MgB_4O_7*: Cu phosphors.* 2009.
68. Furetta, C., S. Guzmán, and E. Cruz-Zaragoza, *The Initial Rise Method in the case of multiple trapping levels.* 2009.
69. Karmakar, M., *On the initial rise method for kinetic analysis in thermally stimulated luminescence*. Indian Journal of Science and Technology, 2012. **5**(11): p. 3674-3677.
70. Rawat, N., et al., *Use of initial rise method to analyze a general-order kinetic thermoluminescence glow curve.* Nuclear Instruments and Methods in Physics Research Section B: Beam Interactions with Materials and Atoms, 2009. **267**(20): p. 3475-3479.
71. Bos, A., *High sensitivity thermoluminescence dosimetry.* Nuclear Instruments and Methods in Physics Research Section B: Beam Interactions with Materials and Atoms, 2001. **184**(1-2): p. 3-28.
72. Chen, R. and Y. Kirsh, *The analysis of thermally stimulated processes*, 2013: Elsevier.

73. Halperin, A. and A. Braner, *Evaluation of thermal activation energies from glow curves.* Physical Review, 1960. **117**(2): p. 408.
74. Basun, S., et al., *The analysis of thermoluminescence glow curves.* Journal of Luminescence, 2003. **104**(4): p. 283-294.
75. Chen, R., J. Lawless, and V. Pagonis, *Two-stage thermal stimulation of thermoluminescence.* Radiation Measurements, 2012. **47**(9): p. 809-813.
76. Chen, R., *On the calculation of activation energies and frequency factors from glow curves.* Journal of Applied Physics, 1969. **40**(2): p. 570-585.
77. Chen, R., *On the analysis of thermally stimulated processes.* Journal of Electrostatics, 1977. **3**(1-3): p. 15-24.
78. Kitis, G., J. Gomez-Ros, and J. Tuyn, *Thermoluminescence glow-curve deconvolution functions for first, second and general orders of kinetics.* Journal of Physics D: Applied Physics, 1998. **31**(19): p. 2636.
79. Kitis, G. and J. Gomez-Ros, *Thermoluminescence glow-curve deconvolution functions for mixed order of kinetics and continuous trap distribution.* Nuclear Instruments and Methods in Physics Research Section A: Accelerators, Spectrometers, Detectors and Associated Equipment, 2000. **440**(1): p. 224-231.
80. M. Gómez Ros, J. and G. Kitis, *Computerised glow curve deconvolution using general and mixed order kinetics.* Radiation protection dosimetry, 2002. **101**(1-4): p. 47-52.
81. Reddy, J. and K. Murthy. *TLD Instrumentation: A Case Study of PC Controlled TL Reader*. in *Defect and Diffusion Forum*. 2014. Trans Tech Publ.
82. Reddy, J.N., J.N. Reddy, and J.D. Reddy, *PC Controlled TL/OSL Research Reader.*
83. Azorín Nieto, J. *Thermoluminescence dosimetry (TLD) and its application in medical physics*. in *AIP Conference Proceedings*. 2004. AIP.
84. Donya, M., et al., *Radiation in medicine: Origins, risks and aspirations.* Global Cardiology Science and Practice, 2015: p. 57.
85. Murthy, K. *Thermoluminescence and its applications: a review*. in *Defect and Diffusion Forum*. 2014. Trans Tech Publ.
86. Valentin, J., *The recommendations of the international commission on radiological protection*, 2007: Elsevier Oxford.

87. Kortov, V., *Materials for thermoluminescent dosimetry: Current status and future trends.* Radiation Measurements, 2007. **42**(4-5): p. 576-581.
88. Murthy, K. *Applications of TLDS in Radiation Dosimetry*. in *Defect and Diffusion Forum*. 2013. Trans Tech Publ.
89. Efremenkov, V., *Radioactive waste management at nuclear power plants.* IAEA Bulletin, 1989. **31**(4): p. 37-42.
90. on Earth, D. and N.R. Council, *Effluent Releases from Nuclear Power Plants and Fuel-Cycle Facilities,* 2012.
91. Kry, S.F., et al., *AAPM TG 158: Measurement and calculation of doses outside the treated volume from external-beam radiation therapy.* Medical physics, 2017. **44**(10): p. e391-e429.
92. Aitken, M.J., D. Zimmerman, and S.J. Fleming, *Thermoluminescent dating of ancient pottery.* Nature, 1968. **219**(5153): p. 442.
93. Wintle, A.G., *Fifty years of luminescence dating.* Archaeometry, 2008. **50**(2): p. 276-312.
94. Sabtu, S.N., et al., *Thermoluminescence dating analysis at the site of an ancient brick structure at Pengkalan Bujang, Malaysia.* Applied Radiation and Isotopes, 2015. **105**: p. 182-187.
95. Mandavia, H., et al., *Thermoluminescence Study of Base Materials of Ceramic Tiles.* Eurasian Chemico-Technological Journal, 2011. **13**(1-2): p. 77-80.
96. Sears, D.W., K. Ninagawa, and A.K. Singhvi, *Luminescence studies of extraterrestrial materials: Insights into their recent radiation and thermal histories and into their metamorphic history.* Chemie der Erde-Geochemistry, 2013. **73**(1): p. 1-37.
97. Pollard, A.M. and C. Heron, *Archaeological chemistry*, 2015: Royal Society of Chemistry.
98. Dubey, V., et al., *Thermoluminescence and chemical characterization of natural calcite collected from Kodwa mines.* Research on Chemical Intermediates, 2013. **39**(8): p. 3689-3697.
99. Dubey, V., et al., *TL and PL Study of beta irradiated limestone collected from Semaria mines of CG Basin.* Int. Res. J. Geol. Miner, 2011. **1**(1): p. 012-017.

100. Munyikwa, K., *Luminescence Dating: Applications in Earth Sciences and Archaeology*, in *Luminescence-An Outlook on the Phenomena and their Applications*, 2016, InTech.

101. Patel, N.P., et al., *Luminescence study and dosimetry approach of Ce on an α-$Sr_2P_2O_7$ phosphor synthesized by a high-temperature combustion method.* Luminescence, 2015. **30**(4): p. 472-478.

102. Patel, N.P., et al., *Thermoluminescence kinetic features of Eu^{3+} doped strontium pyrophosphate after beta irradiation.* RSC Advances, 2016. **6**(81): p. 77622-77628.

103. Patel, N.P., et al., *Optimization of luminescence properties of Tb^{3+}-doped α-$Sr_2P_2O_7$ phosphor synthesized by combustion method.* 2016, Rare Metals: p. 1-7.

104. Murthy, K., et al., *Compact fluorescent lamp phosphors in accidental radiation monitoring.* Radiation protection dosimetry, 2006. **120**(1-4): p. 238-241.

105. Edgar, A., *Luminescent Materials*, in *Springer Handbook of Electronic and Photonic Materials*, 2017, Springer. p. 1-1.

106. Luo, H., A.J. Bos, and P. Dorenbos, *Controlled Electron–Hole Trapping and Detrapping Process in $GdAlO_3$ by Valence Band Engineering.* The Journal of Physical Chemistry C, 2016. **120**(11): p. 5916-5925.

107. Murthy, K., et al., *Thermoluminescence dosimetric characteristics of beta irradiated salt.* Radiation protection dosimetry, 2006. **119**(1-4): p. 350-352.

108. Lu, C.-H. and S. Godbole, *Synthesis and characterization of ultraviolet-emitting cerium-ion-doped $SrBPO_5$ phosphors.* Journal of materials research, 2004. **19**(8): p. 2336-2342.